

Light Field Salient Object Detection: A Review and Benchmark

Yao Jiang, Tao Zhou, Ge-Peng Ji, Keren Fu*, Qijun Zhao, and Deng-Ping Fan

Abstract—Salient object detection (SOD) is a long-standing research topic in computer vision and has drawn an increasing amount of research interest in the past decade. Since the light field records more comprehensive and complete information of natural scenes that benefits SOD in a number of ways, using the light field input to improve saliency detection over the conventional single RGB input is an emerging trend. This paper provides the first comprehensive review and benchmark for SOD on light field, which has long been lacking in the saliency community. Firstly, we introduce the preliminary knowledge of light field including theory and data forms, and then review existing studies on light field SOD, covering ten traditional models, six deep learning-based models, one comparative study, and one brief review. Existing datasets for light field SOD are summarized with detailed information and statistical analysis. Secondly, we benchmark seven representative light field SOD models together with several cutting-edge RGB-D SOD models on four widely used light field datasets, from which insightful discussions and analyses including the comparison between light field SOD and RGB-D SOD models are achieved. Besides, due to the inconsistency of datasets in their current forms, we further generate complete data and supplement focal stacks, depth maps and multi-view images for the inconsistent datasets, making them consistent and unified. Our supplemented data makes a universal benchmark possible. Lastly, because light field SOD is a quite special problem attributed to its diverse data representations and high dependency on acquisition hardware, making it differ greatly from other saliency detection tasks, we provide nine hints into the challenges and future directions, and outline several open issues. We hope our review and benchmarking could serve as a catalyst to advance research in this field. All the materials including collected models, datasets, benchmarking results, and supplemented light field datasets will be publicly available at our project site <https://github.com/kerenfu/LFSOD-Survey>.

Index Terms—Light field, salient object detection, deep learning, benchmarking.

I. INTRODUCTION

SALIENT object detection (SOD) [1] is a fundamental task in computer vision, aiming at detecting and segmenting the most human-eye-attracting regions or objects. SOD is a sub-field of saliency detection, whereas the other sub-field is called eye fixation prediction [2]–[5], whose goal is to predict where human look in a scene. SOD plays an important role and has wide applications in computer vision, computer graphics,

Y. Jiang, K. Fu and Q. Zhao are with the College of Computer Science, Sichuan University, China. (Email: yaojiangyj@foxmail.com, fkrsuper@scu.edu.cn, qjzhao@scu.edu.cn).

T. Zhou and D.-P. Fan are with the Inception Institute of Artificial Intelligence (IIAI), Abu Dhabi, UAE. (Email: taozhou.ai@gmail.com, dengpfan@gmail.com).

G.-P. Ji is with the School of Computer Science, Wuhan University, China. (Email: gepengai.ji@gmail.com)

Corresponding author: Keren Fu.

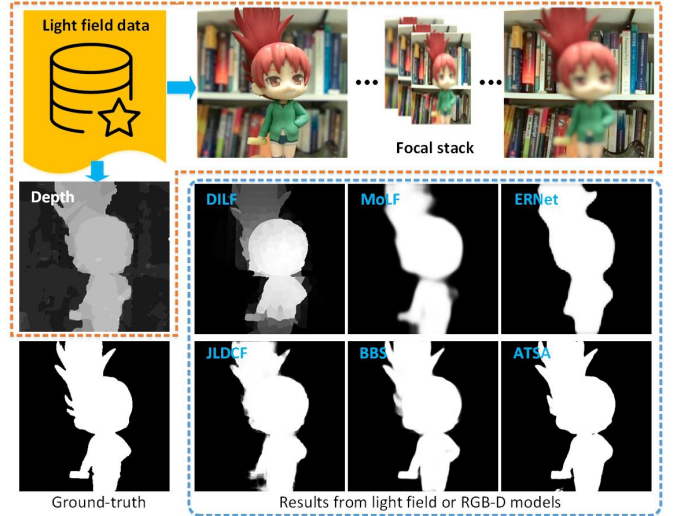


Fig. 1: Salient object detection on a sample scenario using three light field based (*i.e.*, DILF [25], MoLF [26] and ERNet [27]) and three state-of-the-art RGB-D based SOD models (*i.e.*, JLDCF [28], BBS [29], and ATSA [30]).

and robotics. For example, in computer vision, it is used in image retrieval [6], object detection and recognition [7]–[10], semantic segmentation [11]–[13] and unsupervised video object segmentation [14], [15]. In computer graphics, example applications include non-photorealist rendering [16], automatic image cropping [17], image re-targeting [18] and video summarization [19], [20]. In robotics, SOD assists human-robot interaction [21], [22] and object discovery [23], [24].

In recent years, deep learning-based SOD has shown great potentials in achieving promising performance, and attracted increasing research concerns. However, SOD based on single modality (*i.e.*, detection on a single RGB input image) still encounters several challenges in complex scenarios, such as heavy background clutter [31], high similarity between foreground and background. To solve these challenges, incorporating additional supplementary knowledge such as scene depth [28]–[30], [32]–[37] or motion [38] usually has been proven the effectiveness for boosting SOD performance, of which using light field data [25]–[27], [39]–[53] is another emerging trend.

Light field SOD explores how to detect salient objects using light field data as input. In the 3D space, a light field [54] captures all the light rays at every spatial location and in every direction. As a result, it can be viewed as an array of images captured by a grid of cameras towards the scene. Compared

with the RGB images captured by a regular camera or depth maps acquired by a depth sensor, the light field data acquired by a plenoptic camera records more comprehensive and complete information of natural scenes, which covers, for example, depth information [55]–[59], focusness cues [39], [59] as well as angular changes [50], [59]. Therefore, the light field data can benefit SOD in a number of ways. Firstly, the light field has the ability of refocusing after being acquired [59]. This allows to produce a stack of images focusing at different depth, and such focusness cues have been demonstrated useful for SOD [60]. Secondly, a light field can provide images of a scene from an array of viewpoints [61]. Such images of multiple viewpoints have abundant spatial parallax and geometric information. Lastly, depth information of a scene is embedded in light field data and can be estimated from a focal stack or multi-view images by different means as described in [55]–[58]. In this sense, RGB-D data could be deemed as a special degenerated case of the light field data. Fig. 1 shows example results obtained by using light field SOD methods as well as RGB-D SOD models on the light field data (focal stack) and depth data.

Although the light field has great benefits for SOD and was first explored in [39] in 2014, till now, this research area is still under-explored. Specifically, compared with RGB SOD or RGB-D SOD, there are fewer studies on light fields. Despite of this sparsity of literature, existing models vary in technical frameworks as well as used light field datasets. Several light field datasets had been proposed in the past decade. To the best of our knowledge, there is no comprehensive review as well as a benchmark for light field SOD. Regarding this issue, a comparative study was conducted by Zhang *et al.* [53] in 2015. However, they only compare the classic light field SOD model proposed by Li *et al.* [39] with a set of 2D saliency models to show the effectiveness of incorporating light field knowledge. Besides, the evaluation is done only on LFSOD dataset which contains 100 light field images. Recently, Zhou *et al.* [62] briefly summarize existing light field SOD models and related datasets. However, their work is mainly focused on RGB-D based SOD, and only a small part of contents and space is given for reviewing light field SOD, leading to an insufficient review of model details and these related datasets. Besides, they have not benchmarked light field SOD models and provided any performance evaluation. Thus, we believe that the lack of a complete review of the existing models and datasets may somewhat hinder further research in this field.

To this end, in this paper we conduct *the first comprehensive review and benchmark for light field SOD*. We review previous studies on light field SOD, including ten traditional models [25], [39]–[42], [44]–[48], six deep learning-based models [26], [27], [49]–[52], one comparative study [53], and one brief review [62]. Meanwhile, we review existing light field SOD datasets [39], [44], [49], [50], [52], and provide statistical analysis for these datasets, including object size, distance between the object and image center, focal slice numbers, and object numbers. Due to the inconsistency of datasets, for example, some datasets did not provide focal stacks while others lacked depth maps or multi-view images,

we further work on generating complete data and supplement focal stacks, depth maps and multi-view images for some datasets, therefore making them consistent and unified. Besides, we benchmark seven light field SOD models [25]–[27], [39], [40], [50], [52] whose results/codes are available, together with several cutting-edge RGB-D SOD models [28]–[30], [32]–[37], discussing the connection between the two and providing insight into the challenges and future directions. All the materials involved in this paper, including collected models, benchmark datasets, and results, supplemented light field data, source code links, will be publicly available at <https://github.com/kerenfu/LFSOD-Survey>. The main contributions of this paper are four-fold:

- We provide the first systematic review regarding light field SOD, including models and datasets. Such a survey has long been lacking in the saliency community and is helpful for encouraging future research in this area.
- We conduct analysis on the property of different datasets. As some datasets lacked data of certain aspects, *e.g.*, focal stacks, multi-view images, we generate more data from existing datasets as supplement, making them more complete and unified. This will also facilitate future research in this area.
- We further benchmark seven light field SOD models together with several cutting-edge RGB-D SOD models on the datasets with our supplemented data, and provide insightful discussions.
- We investigate several challenges for SOD on light fields and discuss the relation to other topics, shedding light on the challenges and directions for future work.

The remainder of the paper is organized as follows. We will review the preliminaries of the light field, existing models and datasets for light field SOD, and provide related discussions and analyses in Section II. In Section III, we describe the evaluation metrics used as well as benchmark results. We then discuss future research directions and outline several open issues of this field in Section IV. Finally, we draw the conclusion in Section V.

II. PRELIMINARIES, MODELS AND DATASETS

In this section, we first briefly introduce the theory of light field, the data form of it, and how it has been used for SOD. We then review the prior works on light field SOD, roughly categorizing them into traditional models *vs.* deep learning-based models. Finally, we summarize datasets explored for light field SOD and review their detailed information.

A. Light Field

1) *Light Field and Light Field Camera*: A light field [54] consists of all the light rays flowing through every point and in every direction in the 3D space. In 1991, Adelson and Bergen [63] proposed a plenoptic function (P), which uses $P(\theta, \phi, \lambda, t, x, y, z)$ to describe the wavelength λ and time t at any direction (θ, ϕ) on any point (x, y, z) , in order to represent the light field information. In an imaging system, the wavelength and time can be represented by RGB channels and different frames, and light usually propagates in

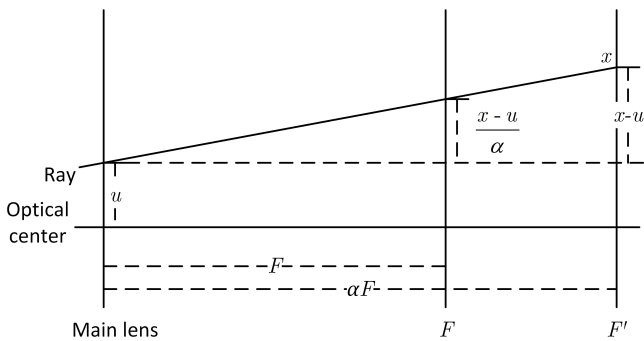


Fig. 4: Illustration of the refocus principle.

be synthesized. Specially, when the angular direction (u^*, v^*) equals to that of the central view, namely (u_0, v_0) , the center-view image is achieved. On the other hand, micro-lens images can be generated by sampling the (x, y) dimensions. Giving a micro-lens location (x^*, y^*) leads to a micro-lens image $L_F(u, v, x^*, y^*)$, which captures multiple perspectives of a scene point. Note that if varying (x^*, y^*) , different micro-lens images can be obtained and all micro-lens images is able to compose a micro-lens image array representing complete light field information. Visualization of micro-lens images and multi-view images can be found in the recent work [52].

Moreover, besides the above-mentioned data forms, the depth map which contains scene depth information can also be estimated from the light field. As mentioned that depth information is embedded in the focusness and angular cues, a depth map can be generated by combining both defocusness and correspondence (angular) cues. More details about depth estimation from light field refer to [55]–[58].

B. Light Field SOD Models and Reviews

In this section, we review existing models proposed for light field SOD, including ten traditional models that resort to hand-crafted features, and six deep learning-based models. Also, one comparative study and one brief review are revisited. Details of all these works are summarized in Table I.

1) Traditional Models:

LFS [39] was the pioneering (also the earliest) work on light field SOD, which started to investigate the problem of using light field data as input for SOD, instead of using conventional RGB images or depth maps. Together with this method, the first light field SOD dataset was constructed. This method first incorporated the focusness measure with location priors to determine the background and foreground slices. Then in the all-focus³ image, it computed the background prior and contrast cues to detect saliency candidates. Finally, a saliency map was generated by incorporating the saliency candidates in the all-focus image with those in the foreground slices, where objectness cues were used to weigh the candidates. An extension of this work was published in [43].

WSC [40] was proposed as a unified framework for 2D, 3D and light field SOD problems, which can handle heterogeneous

³In this paper, “all-focus” and “all-in-focus” are used interchangeably. Their meanings are the same.

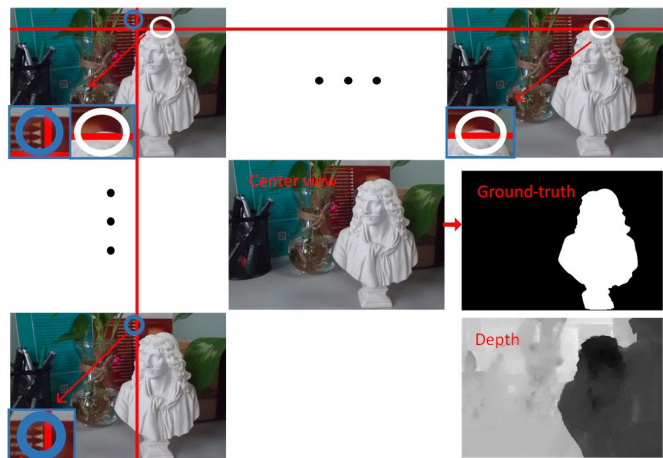


Fig. 5: Multi-view images (including the center-view image), the depth map, and ground-truth. Notice the inconspicuous parallax (disparity) conveyed by the former (zoomed in as the bottom-left in each multi-view image).

types of data. Based on the weighted sparse coding framework, the authors first used a non-saliency dictionary to reconstruct a reference image, where patches with high reconstruction error were selected as the saliency dictionary. This saliency dictionary was later refined by iteratively running the weighted sparse framework to achieve the final saliency map. For the light field case, features used for dictionary construction were derived from the all-focus RGB image, depth map, and also focal stacks.

DILF [25] used global cues in the light field data to measure the saliency of a superpixel. It computed the depth-induced contrast saliency and color contrast saliency from the all-focus image and depth image, which were then used to generate a contrast saliency map. It also computed the background priors based on the focusness measure embedded in the focal stacks and used them as weights to eliminate background distraction and meanwhile enhance the saliency estimation.

RL [41] proposed to estimate the relative locations of scene points by using a filtering process. It designed two filters, namely the foreground and background filter to calculate the relative locations in a raw light field image. Such relative locations, which can be treated as conveying scene depth information, were then incorporated with the robust background detection and saliency optimization framework proposed in [67] to achieve enhanced saliency detection.

BIF [42]. This work used the Bayesian framework to fuse multiple features extracted from RGB images, depth maps and the focal stacks. Inspired by traditional SOD methods, this method utilized boundary connectivity prior, background likelihood scores and color contrast to generate background probability maps, foreground slices, color-based saliency maps and also depth-induced contrast maps. For all the features extracted, it then used a two-stage Bayesian scheme to fuse diverse features.

MA [44] measured the saliency of a superpixel by computing the intra-cue distinctiveness between two superpixels, where features considered include color, depth, and flow

TABLE I: Overview of light field SOD models and review works. Regarding the datasets, please see Table II. About the abbreviations: FS=Focal stacks, DE=Depth maps, MV=Multi-view images, ML=Micro-lens images, OP=Open-source. FS, DE, MV and ML indicate the data forms input to the models. The emerged dataset is highlighted in **bold** in the “Main components”.

	Models	Pub. Year	Training dataset(s)	Testing dataset(s)	Main components	FS	DE	MV	ML	OP
Traditional models	LFS [39]	CVPR 2014	-	LFS	Focusness measure, Location priors, Contrast cues, Background prior, New dataset	✓				✓
	WSC [40]	CVPR 2015	-	LFS	Weighted sparse coding, Saliency/Non-saliency dictionary construction	✓				✓
	DILF [25]	IJCAI 2015	-	LFS	Depth-induced/Color contrast, Background priors by focusness	✓	✓			✓
	RL [41]	ICASSP 2016	-	LFS	Relative locations, Guided filter, Micro-lens images				✓	
	BIF [42]	NPL 2017	-	LFS	Bayesian framework, Boundary prior, Color/Depth-induced contrast	✓	✓			
	LFS [43]	TPAMI 2017	-	LFS	An extension of [39]	✓				✓
	MA [44]	TOMM 2017	-	LFS + HFUT	Superpixels intra-cue distinctiveness, Light-field flow, New dataset	✓	✓	✓		
	SDDF [45]	MTAP 2018	-	LFS	Background priors, Gradient operator, Color contrast, Local binary pattern histograms	✓				
	SGDC [46]	CVPR 2018	-	LFS	Focusness cues, Color and depth contrast	✓	✓			
	RDFD [47]	MTAP 2020	-	LFS	Region-based depth feature descriptor, Dark channel prior, Multi-layer cellular automata	✓				
	DCA [48]	TIP 2020	-	LFS	Depth-induced cellular automata, Object-guided depth	✓	✓			
Deep learning models	DLLF [49]	ICCV 2019	DUT-LF	LFS + DUT-LF	VGG-19, Attention sub-network, ConvLSTM, Adversarial examples, New dataset	✓				
	DLSD [50]	IJCAI 2019	DUT-MV	DUT-MV	View synthesis network, Multi-view detection/attention, VGG-19, New dataset			✓		✓
	MoLF [26]	NIPS 2019	DUT-LF	HFUT + LFS + DUT-LF	VGG-19, Memory-oriented spatial fusion, Memory-oriented feature integration	✓				✓
	ERNet [27]	AAAI 2020	DUT-LF + HFUT	HFUT + LFS + DUT-LF	VGG-19, ResNet-18, Multi-focusness recruiting/screening modules, distillation	✓				✓
	LFNet [51]	TIP 2020	DUT-LF	HFUT + LFS + DUT-LF	VGG-19, Refine unit, Attention block, ConvLSTM	✓				
	LFDCN [52]	TIP 2020	Lytro Illum	Lytro Illum + HFUT + LFS	Micro-lens images/image arrays, DeepLabv2, Model angular changes, New dataset				✓	✓
Reviews	CS [53]	NEURO 2015	-	LFS	Comparative study between 2D vs. light field saliency					
	RGBDS [62]	CVM 2020	-	-	In-depth RGB-D SOD survey, Brief review of light field SOD					

inherited from different focal planes and multiple viewpoints. The light-field flow was first employed in this method, and was estimated from focal stacks and multi-view sequences to capture depth discontinuities/contrast. The saliency measure was later enhanced by location prior and a random-search-based weighting strategy. In addition, the authors proposed a new light field SOD dataset, which was the largest at that time.

SDDF [45] made use of depth information embedded in focal stacks to conduct accurate saliency detection. Background measurement was first obtained by applying a gradient operator to focal stack images, and the focal slice with the highest measurement was chosen as the background layer. Coarse prediction was generated by separating the background and foreground in the all-focus image through the derived background regions, and the final saliency map was globally calculated via both color and texture (local binary pattern histograms) contrast based on the coarse saliency map.

SGDC [46]. This work presented a light field SOD approach named contrast-enhanced saliency detection for optimizing the multi-layer light field display. It first computed a super-pixel level focusness map for each re-focus image and then chose the re-focus image with the highest background likelihood score to derive background cues. Such focusness background

cues were later incorporated with color and depth contrast saliency. The final results were optimized by the optimization framework proposed in [67].

RDFD [47] addressed the light field SOD problem via a multiple-cue integration framework. A region-based depth feature descriptor (RDFD) defined over the focal stack was proposed, which was based on the observation that dark channel prior can be used to estimate the degree of defocusing/blurriness. The RDFD was generated by integrating the degrees of defocusing over all focal stack images, alleviating the limitation on requiring accurate depth maps. RDFD features were used to compute a region-based depth contrast map and a 3D spatial distribution prior. These cues were merged into a single map using a multi-layer cellular automata (MCA).

DCA [48]. As a recent work, this paper proposed a depth-induced cellular automata (DCA) for light field SOD. The inputs of the model included an all-focus image, a depth map and a focal stack. Firstly, it used the focusness and depth cue to calculate the object-guided depth map and select background seeds. Based on the seeds, a contrast saliency map was computed and multiplied with the object-guided depth map to achieve a depth-induced saliency map, which was subsequently optimized by DCA. Finally, the optimized map

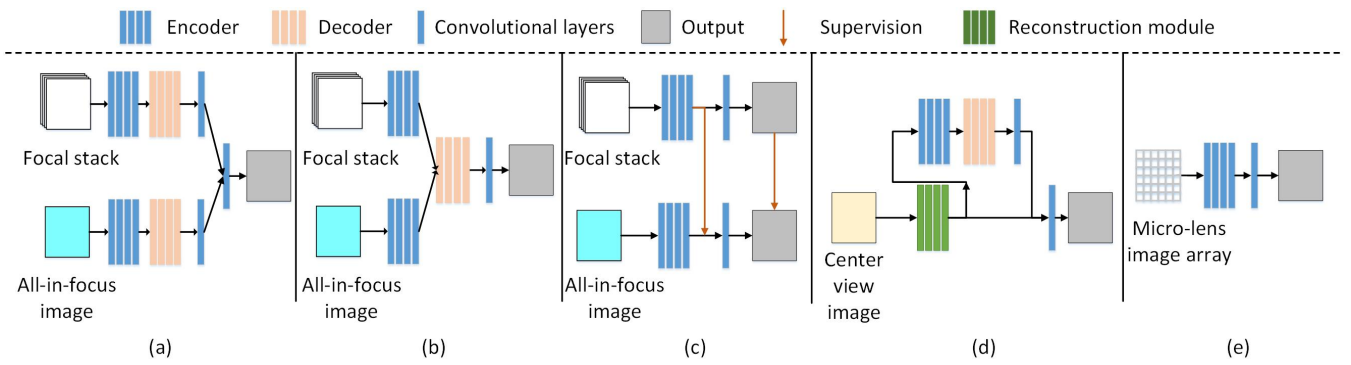


Fig. 6: Frameworks of deep light field SOD models. (a) Late-fusion (DLLF [49]). (b) Middle-fusion (MoLF [26], LFNet [51]). (c) Knowledge distillation-based (ERNet [27]). (d) Reconstruction-based (DLSD [50]). (e) Single-stream (LFDCN [52]). Note (a)-(c) utilize the focal stack and all-focus image, whereas (d)-(e) utilize the center-view image and micro-lens image array.

was combined with the depth-induced saliency map, and a Bayesian fusion strategy and CRF were employed to further refine the result.

Summary of Traditional Models. As summarized in Table I, traditional SOD models on light fields often extend various hand-crafted features/hypotheses which are widely adopted in conventional saliency detection, such as color contrast, background priors, object location cues. Some features specially tailored for light fields, like focusness, depth, and light-field flow, are also considered. Besides, these models tend to employ post-refinement steps *e.g.*, the optimization framework [25], [41], [44], [46], [48] and CRF [48] to achieve saliency maps with more accurate boundaries. Despite of this, due to the general limitation of using hand-crafted features, traditional SOD models can hardly generalize well in challenging scenarios. Regarding the data forms leveraged by traditional models, almost all of them work with focal stacks, while depth is incorporated by some of them, and very few models consider the multi-view [44] and micro-lens data [41] from light field. One can see that due to the limitation of datasets in the early time, most traditional models are only evaluated on LFSD dataset.

2) Deep Learning-based Models:

DLLF [49]. This paper proposed a two-stream fusion framework which explored focal stacks and all-in-focus images separately. In the focal stack stream, DLLF first extracted features from cascaded focal slices through a fully convolutional network. Diverse features from different slices were then integrated by a recurrent attention network, which employed attention sub-network and ConvLSTM [68] to adaptively incorporate weighted features of slices and exploit their spatial relevance. Finally, the fused features were fed to convolutional layers to generate a saliency map for the focal stack stream. This map was combined with the other saliency map derived from the all-in-focus image to generate the final saliency map. In addition, to improve the robustness of the proposed network, the authors generated adversarial examples by adding noise into training images. In addition, to address the limitation of data for training deep networks, a new large dataset was introduced for light field SOD.

DLSD [50] treated light field SOD as two sub-problems,

light field synthesis from a single-view image and light-field-driven SOD. This model first employed a light field synthesis network, which estimated depth maps along horizontal and vertical directions with two independent convolutional networks. According to the depth maps, the single-view image was warped into horizontal and vertical viewpoints of light field. After the light field images were constructed, a light-field-driven SOD network, consisting of two parts: multi-view saliency detection sub-network and multi-view attention module, was designed to make a saliency prediction. Generally, this model indeed inferred a saliency map from a 2D single-view image, but utilized the light field (the multi-view data form) as the middle bridge. To train the model, a new dataset containing multi-view images and a pixel-wise ground-truth of central view was introduced.

MoLF [26]. To better exploit spatial information and comprehensively integrate multi-level features, the authors proposed a memory-oriented spatial fusion module (Mo-FSM) and feature integration module (Mo-FIM). Mo-FSM utilized attention mechanism to learn the importance of different feature maps and a ConvLSTM [68] to gradually refine the spatial information. A global perception module (GPM) was used to capture global contextual information of the fused feature maps. For Mo-FIM, a scene context integration module (SCIM) and ConvLSTM [68] were employed to learn channel attention maps and exploit their spatial information. Besides, MoLF extracted the focal stack and all-in-focus image features with two separate networks.

ERNet [27]. The computation-and-memory issue is an urgent problem in light field SOD since high dimensional light field data is used. To address this, the authors proposed a two-stream teacher-student network based on knowledge distillation. The teacher stream used a multi-focusness recruiting module (MFRM) and a multi-focusness screening module (MFSM) to recruit and distill knowledge from focal slices, while the student network took a single RGB image as input to achieve computational efficiency. In this scheme, the student stream was supervised by the saliency maps obtained from the teacher stream.

LFNet [51]. In this paper, the authors proposed a two-stream fusion network to better refine the complementary

TABLE II: Overview of light field SOD datasets. About the abbreviations: MOP=Multiple-Object Proportion (The percentage of images regarding the entire dataset, which have more than one objects per image), FS=Focal Stacks, DE=Depth maps, MV=Multi-view images, ML=Micro-lens images, GT=Ground-truth, Raw=Raw light field data. FS, MV, DE, ML, GT and Raw indicate the data provided by the datasets.

Dataset	Scale	Spatial resolution	Angular resolution	MOP	FS	MV	DE	ML	GT	Raw	Device
LFSD [39]	100 (No official split)	360×360	-	0.04	✓		✓		✓	✓	Lytro
HFUT [44]	255 (No official split)	328×328	7×7	0.29	✓	✓	✓		✓		Lytro
DUT-LF [49]	1462 (1000 train, 462 test)	600×400	-	0.05	✓		✓		✓		Lytro Illum
DUT-MV [50]	1580 (1100 train, 480 test)	400×590	7×7	0.04		✓			✓		Lytro Illum
Lytro Illum [52]	640 (No official split)	540×375	9×9	0.15				✓	✓	✓	Lytro Illum

information and integrate the focusness and blurriness information which changed gradually in focal slices. LFNet used two separate networks to extract features from the all-focus image and focal stack, and fed those features to a light field refinement module (LFRM) and integration module (LFIM) to generate a final saliency map. In LFRM, feature maps extracted from a single focal slice were fed to a refine unit to learn the residuals. Then, it fused with the all-in-focus features to refine the saliency map using the supplementary information from the focal stack and all-focus image. LFIM used an attention block to adaptively incorporate features of each slice with different weights, and also a ConvLSTM [68] to exploit the spatial relevance of the attentive features.

LFDCN [52] was proposed as an end-to-end deep convolutional network for light field SOD with micro-lens image arrays as input. Firstly, LFDCN adopted a MAC (Model Angular Changes) block tailored to model angular changes in each local micro-lens image and then fed the extracted features to a modified DeepLab-v2 [69] network, capturing multi-scale information and long-range spatial dependencies. Specifically, the authors proposed three variants of MAC blocks, and showed that the MAC block with kernel size the same as the angular resolution achieved the best performance. Together with the model, a new Lytro Illum dataset which included high-quality micro-lens image arrays was proposed.

Summary of Deep Models. As summarized in Table I, most deep models take the focal stack as network input. Due to the multi-variable property of focal stacks, modules such as attention mechanisms [26], [27], [49]–[51] and ConvLSTMs [26], [27], [49], [51] are preferred. Some deep models consider other data forms beyond the focal stack, like the multi-view image [50] and micro-lens image array [52], which often lead to different network designs. The limitation of datasets is somewhat alleviated in the deep learning era, as three new datasets are introduced to better train deep neural networks.

Since using deep learning-based schemes for light field SOD is the leading trend, we categorize existing deep models into five categories as illustrated in Fig. 6. The late-fusion scheme (Fig. 6 (a)) aims at individual predictions from the input focal stack and all-focus image, and then simply fuse the results. The middle-fusion (Fig. 6 (b)) extracts features from the focal stack and all-focus image in a two-stream manner. Fusion across features is done by an elaborately designed decoder. The knowledge distillation-based scheme (Fig. 6 (c)) uses both the features and prediction from the focal stack stream to supervise those features and prediction obtained from the all-focus stream, effectively boosting the performance of the

latter. The reconstruction-based (Fig. 6 (d)) reconstructs light field data/information from a single input image. With the assistance of the reconstructed light field, an encoder-decoder architecture is adopted to complete light field SOD. Finally, the single-stream scheme (Fig. 6 (e)) processes the micro-lens image array directly by using a single bottom-up stream to obtain the final prediction.

3) Other Review Works:

CS [53]. This paper provided a comparative study between light field saliency and 2D saliency, showing the advantage of conducting SOD task on light field data over using single 2D image data. It compared the classical model LFS [39] on LFSD [39] with eight 2D saliency models. Five evaluation metrics were used in the paper to show that the light field saliency model achieved better and more robust performance than models based on conventional 2D images.

RGBDS [62]. This paper conducted an in-depth and comprehensive survey on RGB-D salient object detection. It reviewed existing RGB-D SOD models from various perspectives, as well as the related benchmark datasets in detail. Considering the relevance that the light field can also provide depth maps, the authors also briefly reviewed the light field SOD models and datasets. However, because the main focus of this paper was RGB-D SOD, only a small part of contents and space was arranged for reviewing the light field SOD, and no associated benchmarking was conducted.

C. Light Field SOD Datasets

Till now, there are in total five datasets introduced for the light field SOD task, including LFSD [39], HFUT [44], DUT-LF [49], DUT-MV [50], and Lytro Illum [52]. We summarize details of these datasets in Table II and show some samples on four datasets (*i.e.*, LFSD, HFUT, Lytro Illum, and DUT-LF) in Fig. 7. Brief introduction is given as following:

LFSD⁴ [39] is the first light field dataset collected for SOD, which contains 60 indoor and 40 outdoor scenes. This dataset is captured by Lytro camera and provides a focal stack, all-in-focus image, depth map and the corresponding ground-truth for each light field. The image spatial resolution is 360×360 . Besides, raw light field data is also available in LFSD. Note that most images in this dataset contain one single center-placed objects with relatively simple background.

HFUT⁵ [44] contains 255 light fields with both indoor and outdoor scenes. Each light field contains focal slices whose

⁴<https://sites.duke.edu/nianyi/publication/saliency-detection-on-light-field/>

⁵<https://github.com/pencilzhang/MAC-light-field-saliency-net>

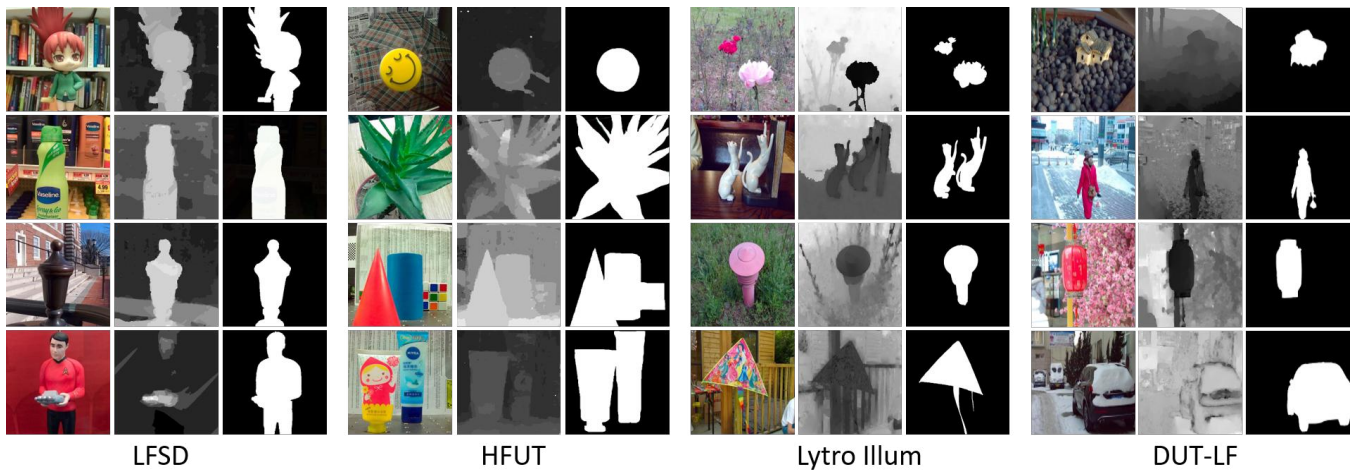


Fig. 7: Examples of RGB images, depth, and ground-truth (GT) from four datasets: LFSD [39], HFUT [44], Lytro Illum [52] and DUT-LF [49]. In each group, RGB images, depth maps and GT are shown from left to right.

slice number varies from 2 to 13. The angular resolution is 7×7 and the spatial resolution is 328×328 . Notably, focal stacks, all-in-focus images, multi-view images and coarse depth maps are all provided in this dataset. Several challenges regarding SOD, *e.g.*, occlusions, cluttered background and appearance changes, are presented in HFUT.

DUT-LF⁶ [49] is one of the largest light field SOD dataset to date, which contains 1462 light fields in total. It is acquired by a Lytro Illum camera in both indoor and outdoor scenes. The entire dataset is officially divided into 1000 training samples and 462 testing samples. All-focus images, focal stacks and the corresponding ground-truth are provided for different light fields. The slice number of a focal stack ranges from 2 to 13, and the image spatial resolution is 600×400 . It is worth nothing that DUT-LF has covered various challenges like different types of objects, low appearance contrast between salient objects and their background, and varied object locations.

DUT-MV⁷ [50] is another large-scale light field dataset for SOD, which is generated from the same database as DUT-LF (with 1081 scenes identical). In contrast to other datasets, this dataset is proposed for better exploiting the angular cues. Therefore, only multi-view images with respect to horizontal and vertical viewpoints are available, together with the ground-truth of the center view image. DUT-MV contains 1580 light fields in total, and is officially divided into training and testing set with 1100 and 480 samples, respectively. The spatial resolution of each image is 400×590 and the angular resolution is 7×7 .

Lytro Illum⁵ [52] contains 640 high-quality light fields captured by a Lytro Illum camera and the images in this dataset vary significantly in object sizes, texture, background clutter and illumination. Lytro Illum provides center-view images, micro-lens image arrays, raw light field data as well as the corresponding ground-truth of the center-view images. The resolution of micro-lens image arrays is 4860×3375 , while

center-view images and ground-truth have a 540×375 spatial resolution. The angular resolution can be inferred as 9×9 .

Dataset Analysis. From the summarization in Table II, we can observe two issues existed, namely scale limitation and non-unified data forms. Compared to the large datasets constructed for the conventional SOD task, such as DUT-OMRON (5,168 images) [70], MSRA10K (10,000 images) [1] and DUTS (15,572 images) [71], the existing light field SOD datasets are still small, probably making it difficult to evaluate data-driven models and also insufficient to train deep networks. Besides, their data forms are not always identical. For example, Lytro Illum does not provide focal stacks, while DUT-LF/DUT-MV only provides focal stacks/multi-view images without offering the raw data. This makes comprehensive benchmarking very difficult, because a model using focal stacks as input cannot run on DUT-MV and Lytro Illum. We will show how we alleviate this problem in Section III-B, and also discuss the underlying future direction in Section IV.

For better understanding the above-mentioned datasets, we have conducted statistical analysis, including size ratios of salient objects, distributions of normalized object distances from image centers, numbers of focal slices and numbers of objects. The quantitative results are shown in Fig. 8 and Fig. 9. From Fig. 8 (a), we can see that most objects from these datasets have size ratios lower than 0.6. HFUT and Lytro Illum have relatively small objects, while LFSD has objects that are in relatively large sizes. Fig. 8 (b) and Fig. 9 clearly show the spatial distribution of objects. From Fig. 9, we can see that all five datasets present strong center bias, and Fig. 8 (b) reveals that objects from Lytro Illum are generally the closest to the image centers (also indicated by Fig. 9).

In addition, the statistics on focal slice numbers are given in Fig. 8 (c). Note that only three datasets, namely LFSD, HFUT, and DUT-LF, have provided focal slices. The numbers of slices vary from 1 to 12 and there are notable differences between different datasets' slice numbers. The slice numbers correspond to the distribution peaks on LFSD, HFUT and DUT-LF are 12, 3, 6, respectively. This is because LFSD often provides richer depth information than the other datasets. Besides, all

⁶https://github.com/OIPLab-DUT/ICCV2019_DeepLightfield_Saliency

⁷<https://github.com/OIPLab-DUT/IJCAI2019-Deep-Light-Field-Driven-Saliency-Detection-from-A-Single-View>

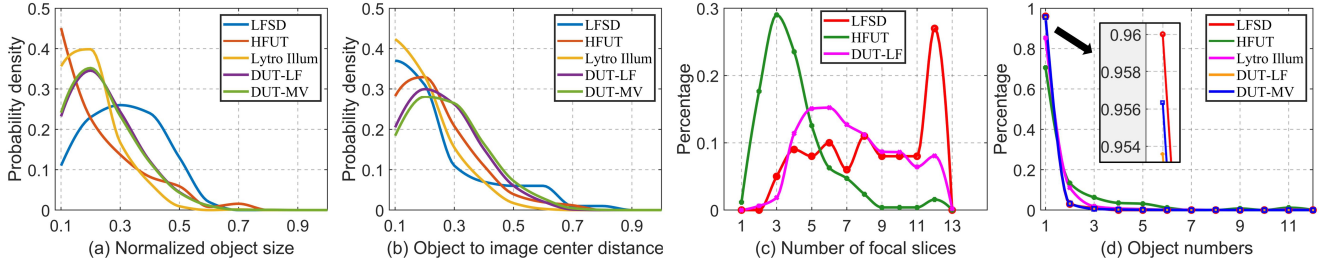


Fig. 8: Statistics of light field datasets, including LFSD [39], HFUT [44], Lytro Illum [52], DUT-LF [49] and DUT-MV [50]. From left to right: (a) distribution of the normalized object size, (b) distribution of the normalized distance between the object and image center, (c) statistics on focal slice numbers, and (d) statistic on object numbers.

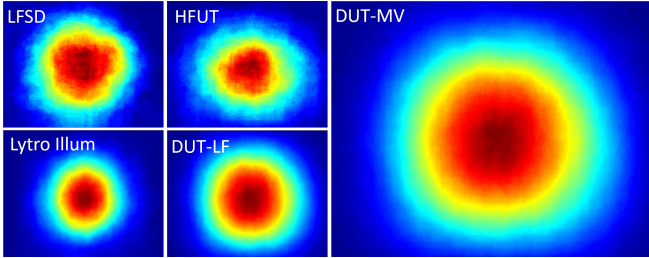


Fig. 9: Object location distribution maps of five datasets (warmer color means higher probability). The maps are computed by averaging ground-truth masks.

three datasets have various slices numbers, indicating that a light field SOD model which resorts to focal stacks should be able to handle various numbers of input slices. Lastly, from Fig. 8 (d), it can be seen that most images from these datasets have a single object per image. Also, HFUT and Lytro Illum have some images with multiple objects (with higher ‘‘MOP’’ in Table II), which could be useful for evaluating models with related purposes.

III. MODEL EVALUATION AND BENCHMARK

In this section, we first review five popular evaluation metrics, and then provide a pipeline to achieve dataset unification. Moreover, we carry out a benchmarking evaluation and provide experimental result analysis.

A. Evaluation Metrics

In our benchmarking of light field SOD models, we employ five kinds of metrics, which are universally agreed and are described as follows:

Precision-recall (PR) [1], [4], [72] curve is defined as:

$$Precision(T) = \frac{|M^T \cap G|}{|M^T|}, Recall(T) = \frac{|M^T \cap G|}{|G|} \quad (3)$$

where M^T is a binary mask obtained by thresholding the saliency map with threshold T , and $|\cdot|$ means the total area of mask. G denotes the ground-truth. A comprehensive precision-recall curve is obtained by changing T from 0 to 255.

F-measure (F_β) [1], [4], [72] is defined as the harmonic-mean of precision and recall:

$$F_\beta = \frac{(1 + \beta^2) Precision \cdot Recall}{\beta^2 \cdot Precision + Recall} \quad (4)$$

where β is the weight between *Precision* and *Recall*, and β^2 is often set to 0.3 to emphasize more on precision. Since Different F-measure-recall pairs, in this paper, we report the maximum F-measure (F_β^{\max}) and mean F-measure (F_β^{mean}) computed from the PR curve. Besides, we also report the adaptive F-measure (F_β^{adp}) [72], whose threshold is computed as the twice of the mean of a saliency map.

Mean Absolute Error (M) [73] is defined as:

$$M = \frac{1}{N} \sum_{i=1}^N |S_i - G_i| \quad (5)$$

where S_i and G_i denote the values at i -th pixel in the saliency map and ground-truth map. N is the total number of pixels in the either map.

S-measure (S_α) [74], [75] is proposed to measure the spatial structure similarities between the saliency map and ground-truth. It is defined as:

$$S_\alpha = \alpha * S_o + (1 - \alpha) * S_r \quad (6)$$

where S_o and S_r denote the object-aware structural similarity and region-aware structural similarity, and α is the parameter balancing between S_o and S_r . In this paper, we set $\alpha = 0.5$ as suggested in [74].

E-measure (E_ϕ) [76] is a recently proposed metric which considers both local and global similarity between the prediction and ground-truth. It is defined as:

$$E_\phi = \frac{1}{w * h} \sum_{i=1}^w \sum_{j=1}^h \phi(i, j) \quad (7)$$

where $\phi(\cdot)$ denotes the enhanced alignment matrix [76]. w and h are the width and height of the ground-truth map, while (i, j) are pixel indexes. Since E_ϕ also performs comparison between two binary maps, we treat it similarly as the F-measure, namely thresholding a saliency map with all possible values and report the maximum and mean E_ϕ , denoted as E_ϕ^{\max} and E_ϕ^{mean} . Besides, adaptive E_ϕ , namely E_ϕ^{adp} , is computed

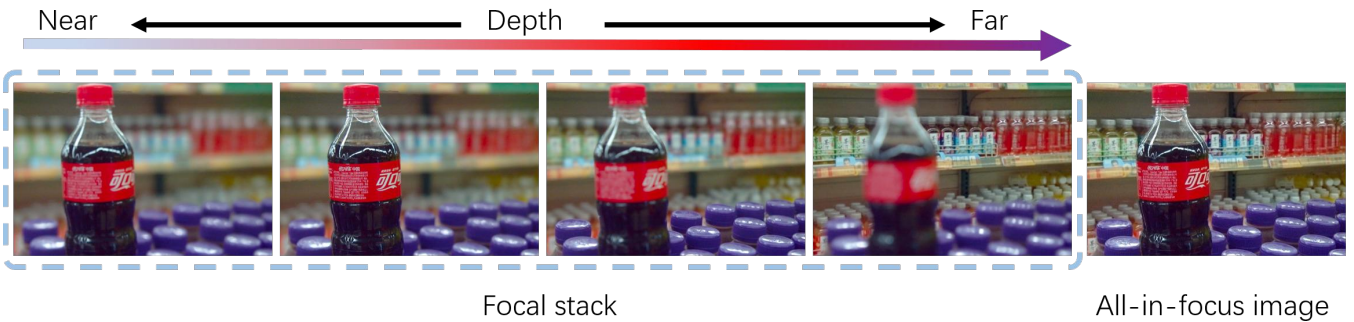


Fig. 10: Example of generated focal slices for Lytro Illum dataset [52], together with the synthesized all-in-focus image.

similarly to the adaptive F-measure mentioned above, where the thresholds are two times the mean saliency values [72].

Regarding the five kinds of metrics, higher PR curves, F_β , S_α and E_ϕ , and lower M indicate better performance.

TABLE III: Datasets unification for light field SOD, which is in contrast to Table II. About the abbreviations: FS=Focal Stacks, DE=Depth maps, MV=Multi-view images, ML=Micro-lens images, Raw=Raw light field data. The data forms marked by “○” mean the data we complete.

Datasets	FS	MV	DE	ML	Raw
LFSD [39]	✓	○	✓	○	✓
HFUT [44]	✓	✓	✓	○	
DUT-LF [49]	✓		✓		
DUT-MV [50]		✓			
Lytro Illum [52]	○	○	○	✓	✓

B. Dataset Unification

As shown in Section II-C and Table II, existing light field SOD datasets face the limitation of non-unified data forms. Such inconsistent data forms makes comprehensive benchmarking difficult. Due to the lack of the data of certain aspects, some models cannot be correctly evaluated on some datasets. To alleviate this issue, we generate more data from existing datasets as supplement, making them more complete and unified. The completed data forms are illustrated in Table III by the circle markers. Furthermore, we will release these data on our project site: <https://github.com/kerenfu/LFSOD-Survey> to facilitate future research in this field.

Generally, we can synthesize various data forms by using the raw light field data, which has been provided by two datasets, *i.e.*, LFSD and Lytro Illum. For Lytro Illum, we generate focal stacks (including all-in-focus images) and depth maps by using the Lytro Desktop software. Regarding focal stack generation, we estimate the approximate focus range for each image scene, and then sample the focal slices within the focus range by an equal step. Some all-blurred or duplicated slices are removed. The number of the final generated focal slices for Lytro Illum ranges from 2 to 16 for each scene, and about 74% scenes have more than 6 slices. Fig. 10 shows an example of the generated focal stack. As mentioned in Section II-A2, multi-view images and micro-lens image array are generated by sampling the light field data in angular and spatial resolution, respectively. So, these two data forms can

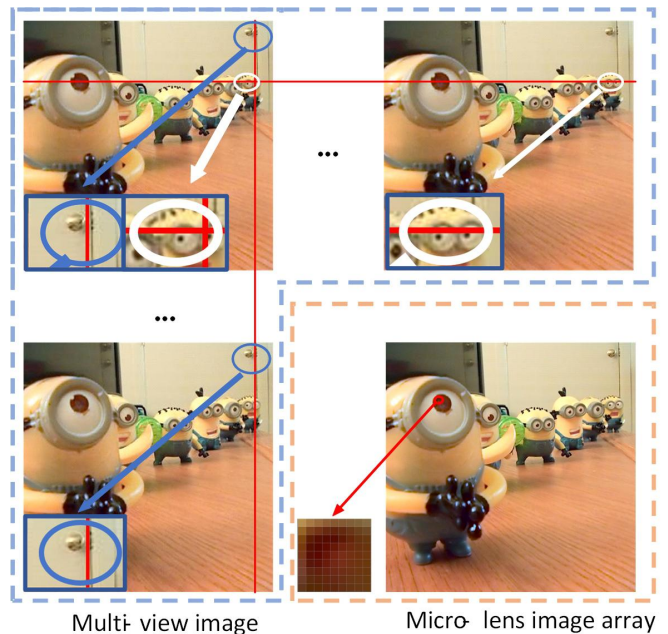


Fig. 11: Example of generated multi-view images (360×360) and micro-lens image array (1080×1080) for LFSD dataset [39]. Same as Fig. 5, the bottom-left of each view image shows zoom-in details to better reflect parallax. The micro-lens image array is composed of many micro-lens images [52].

be transformed between each other. In this way, we generate multi-view images for Lytro Illum from its micro-lens image arrays. We can also synthesize micro-lens image arrays for HFUT through the reverse operation. However, we cannot synthesize micro-lens image arrays for DUT-MV since it has only released the multi-view images in either vertical or horizontal direction. By using the raw data, we supplement multi-view images and micro-lens image arrays for LFSD (Fig. 11). Such complete data makes it possible for more comprehensive model evaluation. For example, models based on focal stacks, such as MoLF and ERNet, now can run and test on Lytro Illum. Note that for the remaining DUT-LF and DUT-MV, supplementing more data is possible in the future if the authors release the raw/more data. If this work has been done, DUT-LF/DUT-MV has the potential to be the *unified training dataset* for future models thanks to its large scale.

TABLE IV: Quantitative measures: S-measure (S_α) [74], max F-measure (F_β^{\max}), mean F-measure (F_β^{mean}) [72], adaptive F-measure (F_β^{adp}) [72], max E-measure (E_ϕ^{\max}), mean E-measure (E_ϕ^{mean}) [76], adaptive E-measure (E_ϕ^{adp}) [72] and MAE (M) [73] of seven light field SOD models (*i.e.*, LFS [39], WSC [40], DILF [25], DLSD [50], MoLF [26], ERNet [27], LFDCN [52]) and nine SOTA RGB-D based SOD models (*i.e.*, BBS [29], JLDCF [28], SSF [32], UCNet [33], D3Net [34], S2MA [35], cmMS [36], HDFNet [37], and ATSA [30]). Note in the table, symbol “N/T” indicates that a model was trained on quite some images from the corresponding dataset, and thus, it is not tested. The top three models are highlighted in red, blue and green. \uparrow/\downarrow denotes that a larger/smaller value is better.

Metric	Light Field SOD Models							RGB-D SOD Models									
	Traditional			Deep learning-based				Deep learning-based									
	LFS [39]	WSC [40]	DILF [25]	DLSD [50]	MoLF [26]	ERNet [27]	LFDCN [52]	BBS [29]	JLDCF [28]	SSF [32]	UCNet [33]	D3Net [34]	S2MA [35]	cmMS [36]	HDFNet [37]	ATSA [30]	
LFS [39]	$S_\alpha \uparrow$	0.681	0.700	0.811	0.786	0.835	0.832	0.782	0.864	0.862	0.859	0.858	0.825	0.837	0.850	0.846	0.858
	$F_\beta^{\max} \uparrow$	0.744	0.743	0.811	0.784	0.834	0.850	0.776	0.858	0.867	0.868	0.859	0.812	0.835	0.858	0.837	0.866
	$F_\beta^{\text{mean}} \uparrow$	0.513	0.722	0.688	0.758	0.809	0.836	0.733	0.842	0.848	0.862	0.848	0.796	0.806	0.850	0.818	0.856
	$F_\beta^{\text{adp}} \uparrow$	0.735	0.743	0.762	0.779	0.819	0.839	0.781	0.840	0.827	0.862	0.838	0.788	0.803	0.857	0.818	0.852
	$E_\phi^{\max} \uparrow$	0.809	0.787	0.861	0.859	0.888	0.886	0.832	0.900	0.902	0.901	0.898	0.863	0.873	0.896	0.880	0.902
	$E_\phi^{\text{mean}} \uparrow$	0.567	0.753	0.741	0.819	0.872	0.883	0.777	0.883	0.894	0.890	0.893	0.850	0.855	0.881	0.869	0.899
	$E_\phi^{\text{adp}} \uparrow$	0.773	0.788	0.821	0.852	0.886	0.887	0.837	0.889	0.882	0.896	0.890	0.853	0.863	0.890	0.872	0.897
	$M \downarrow$	0.205	0.151	0.136	0.117	0.089	0.082	0.127	0.072	0.070	0.067	0.072	0.095	0.094	0.073	0.086	0.068
HFUT [44]	$S_\alpha \uparrow$	0.565	0.613	0.675	0.711	0.742	0.778	0.731	0.751	0.789	0.725	0.748	0.785	0.729	0.723	0.763	0.772
	$F_\beta^{\max} \uparrow$	0.427	0.508	0.595	0.624	0.662	0.722	0.667	0.676	0.727	0.647	0.677	0.671	0.650	0.626	0.690	0.729
	$F_\beta^{\text{mean}} \uparrow$	0.323	0.493	0.513	0.594	0.639	0.709	0.620	0.654	0.707	0.639	0.672	0.651	0.623	0.617	0.669	0.706
	$F_\beta^{\text{adp}} \uparrow$	0.427	0.485	0.530	0.592	0.627	0.706	0.638	0.654	0.677	0.636	0.675	0.647	0.588	0.636	0.653	0.689
	$E_\phi^{\max} \uparrow$	0.637	0.695	0.750	0.784	0.812	0.841	0.797	0.801	0.844	0.816	0.804	0.797	0.777	0.784	0.801	0.833
	$E_\phi^{\text{mean}} \uparrow$	0.524	0.684	0.657	0.749	0.790	0.832	0.733	0.765	0.825	0.763	0.793	0.773	0.756	0.746	0.788	0.819
	$E_\phi^{\text{adp}} \uparrow$	0.666	0.680	0.693	0.755	0.785	0.831	0.772	0.804	0.811	0.781	0.810	0.789	0.744	0.779	0.789	0.810
	$M \downarrow$	0.221	0.154	0.144	0.111	0.094	0.082	0.107	0.089	0.075	0.090	0.090	0.091	0.112	0.097	0.095	0.084
Lytro Illum [52]	$S_\alpha \uparrow$	0.642	0.701	0.712	0.802	0.811	0.822	N/T	0.824	0.831	0.821	0.806	0.818	0.792	0.772	0.801	0.834
	$F_\beta^{\max} \uparrow$	0.529	0.639	0.607	0.753	0.794	0.817	N/T	0.769	0.813	0.776	0.761	0.773	0.739	0.700	0.748	0.796
	$F_\beta^{\text{mean}} \uparrow$	0.377	0.619	0.535	0.712	0.720	0.755	N/T	0.750	0.752	0.763	0.733	0.737	0.704	0.692	0.720	0.766
	$F_\beta^{\text{adp}} \uparrow$	0.528	0.610	0.592	0.709	0.695	0.746	N/T	0.749	0.734	0.763	0.727	0.723	0.698	0.720	0.722	0.760
	$E_\phi^{\max} \uparrow$	0.744	0.807	0.801	0.880	0.903	0.911	N/T	0.884	0.916	0.887	0.890	0.889	0.866	0.858	0.873	0.911
	$E_\phi^{\text{mean}} \uparrow$	0.553	0.794	0.704	0.839	0.865	0.884	N/T	0.870	0.883	0.881	0.872	0.870	0.844	0.814	0.856	0.893
	$E_\phi^{\text{adp}} \uparrow$	0.773	0.795	0.794	0.855	0.852	0.881	N/T	0.886	0.871	0.893	0.872	0.875	0.851	0.870	0.863	0.890
	$M \downarrow$	0.181	0.111	0.129	0.078	0.073	0.064	N/T	0.063	0.064	0.060	0.073	0.066	0.082	0.073	0.075	0.056
DUT-LF [49]	$S_\alpha \uparrow$	0.585	0.657	0.654	N/T	0.887	0.899	0.804	0.865	0.877	0.879	0.831	0.822	0.787	0.804	0.822	0.901
	$F_\beta^{\max} \uparrow$	0.533	0.621	0.585	N/T	0.903	0.908	0.792	0.852	0.878	0.887	0.816	0.797	0.754	0.803	0.801	0.915
	$F_\beta^{\text{mean}} \uparrow$	0.358	0.610	0.492	N/T	0.855	0.891	0.746	0.834	0.846	0.879	0.806	0.776	0.733	0.773	0.776	0.900
	$F_\beta^{\text{adp}} \uparrow$	0.525	0.619	0.597	N/T	0.843	0.885	0.790	0.848	0.835	0.885	0.803	0.784	0.735	0.819	0.778	0.898
	$E_\phi^{\max} \uparrow$	0.711	0.789	0.757	N/T	0.939	0.949	0.863	0.900	0.925	0.922	0.876	0.860	0.839	0.879	0.864	0.941
	$E_\phi^{\text{mean}} \uparrow$	0.511	0.762	0.635	N/T	0.921	0.943	0.806	0.879	0.911	0.907	0.870	0.841	0.817	0.817	0.848	0.937
	$E_\phi^{\text{adp}} \uparrow$	0.742	0.789	0.784	N/T	0.923	0.943	0.872	0.908	0.910	0.918	0.878	0.869	0.842	0.870	0.867	0.938
	$M \downarrow$	0.227	0.149	0.165	N/T	0.051	0.039	0.102	0.066	0.058	0.050	0.081	0.083	0.102	0.079	0.091	0.041

C. Performance Benchmarking and Analysis

To give in-depth understanding of the performance of different models, we conduct the first comprehensive benchmarking of seven light field SOD models (*i.e.*, LFS [39], WSC [40], DILF [25], DLSD [50], MoLF [26], ERNet [27], LFDCN [52]) and nine SOTA RGB-D based SOD models⁸ (*i.e.*, BBS [29], JLDCF [28], SSF [32], UCNet [33], D3Net [34], S2MA [35], cmMS [36], HDFNet [37], and ATSA [30]) on four existing light field datasets including: the entire LFS (100 light fields), HFUT (255 light fields), Lytro Illum (640 light fields) dataset and the testing set (462 light fields) of DUT-LF. Sample images from these datasets are shown in Fig. 7. All the benchmarked models have either publicly available source/executable codes or results provided

⁸The RGB-D SOD models benchmarked in this paper are selected according to the top models concluded by the recent survey [62] and also the latest open-source models published in ECCV-2020. All depth maps fed to a model are not normalized (use their original values) and are optionally reversed on an entire dataset to fit the best performance of this model. All RGB-D SOD models are not re-trained in our experiments, but just use their released model weights trained on RGB-D data. This generally evaluates how well they can generalize to the light field images.

by the authors. Eight evaluation metrics mentioned before (*i.e.*, PR, S-measure, max/mean F-measure, max/mean E-measure, adaptive F-measure and E-measure, mean absolute error) are adopted and the results are reported in Table IV. Meanwhile, the PR curves, max F-measure curves and visual comparisons are shown in Fig. 12, Fig. 13, Fig. 14 Fig. 15. It is worth nothing that the evaluation is not conducted on DUT-MV dataset [50] for it only provides multi-view images, which are not compatible with the input data forms of other light field SOD models. There is one model, namely DLSD [50], not tested on the DUT-LF testing set because it have used quite some images from this dataset for training. Through verification, we find that $\sim 36\%$ of the DUT-LF testing set were used for training the above model. Also, LFDCN is not evaluated on Lytro Illum since the authors conducted five-fold cross-validation on this dataset, and therefore it is not directly comparable to other models. In addition, for ERNet [27], we only evaluate its teacher model since its pre-trained student model is not publicly available. Analyses based on Table IV and Fig. 12 are given as followings.

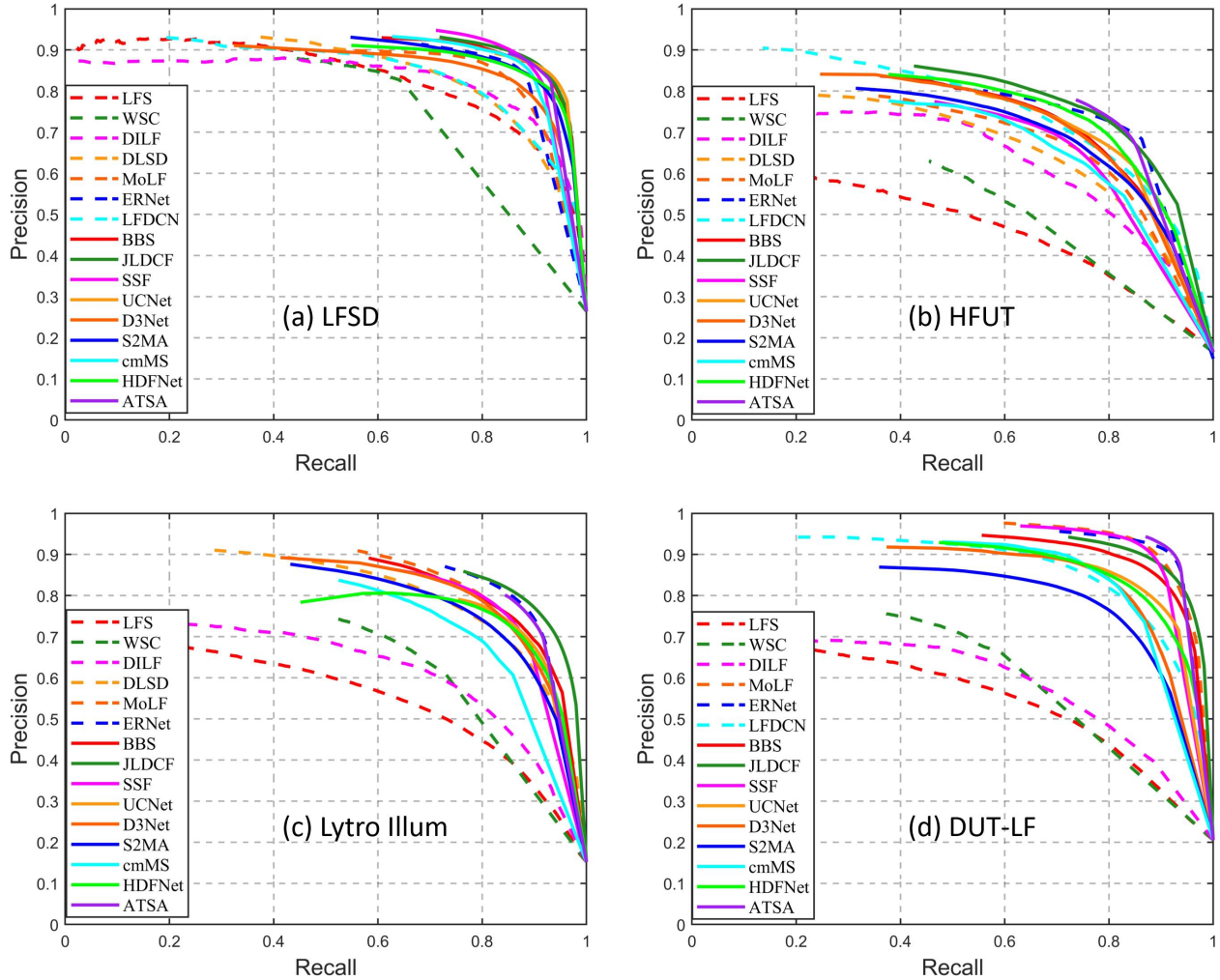


Fig. 12: PR curves on four datasets ((a) LFSD [39], (b) HFUT [44], (c) Lytro Illum [52], and (d) DUT-LF [49]) for seven light field SOD models (*i.e.*, LFS [39], WSC [40], DILF [25], DLSD [50], MoLF [26], ERNet [27], LFDCN [52]) and nine SOTA RGB-D based SOD models (*i.e.*, BBS [29], JLDCF [28], SSF [32], UCNet [33], D3Net [34], S2MA [35], cmMS [36], HDFNet [37], and ATSA [30]). Note that in this figure, the *solid lines* and *dashed lines* represent the PR curves of *RGB-D based SOD models* and *light field SOD models*, respectively.

1) *Traditional vs. deep light field SOD models*: Compare the three traditional models shown in Table I to deep models, one can see that deep learning-based SOD models have significant performance boost on all the datasets. This confirms the power of deep neural networks when applied to this field.

2) *Deep learning-based light field SOD models*: As shown in Table I, MoLF and ERNet adopt focal stacks and all-in-focus images as input data forms, while DLSD and LFDCN use the center-view image and micro-lens image array as input. From Table IV and Fig. 12, it is clearly shown that MoLF and ERNet perform better than DLSD and LFDCN. It is also worth noting that MoLF and ERNet achieve the top-2 performance, which is probably because that the two models were trained on large-scale DUT-LF dataset (*i.e.*, 1000 light fields). Besides, the results indicate that models based on multi-view or micro-lens images are not as effective as those models based on focal stacks. This is probably because that the former are less studied, and the effectiveness of multi-view and micro-lens

images is still under-explored. Moreover, the training data may also matter because LFDCN was trained only on Lytro Illum, which is about twice smaller than DUT-LF. Among the above four models compared, ERNet attains the best accuracy.

3) *Comparison between light field SOD and RGB-D SOD models*: From the quantitative results illustrated in Table IV and Fig. 12, it can be observed that, when applying the latest cutting-edge RGB-D models, they achieve comparable or even better performance than light field SOD models. Three RGB-D models, namely JLDCF, SSF, and ATSA, achieve generally better performance than ERNet on LFSD, HFUT and Lytro Illum. The underlying reasons may be two-fold. First, RGB-D based SOD recently has drawn extensive research interest and many elaborate models are proposed. Inspired by prior research on the RGB SOD problem [77]–[79], these models often pursue edge-preserving results from deep neural networks and employ functional modules/architectures, such as the boundary supplement unit [32], multi-scale feature

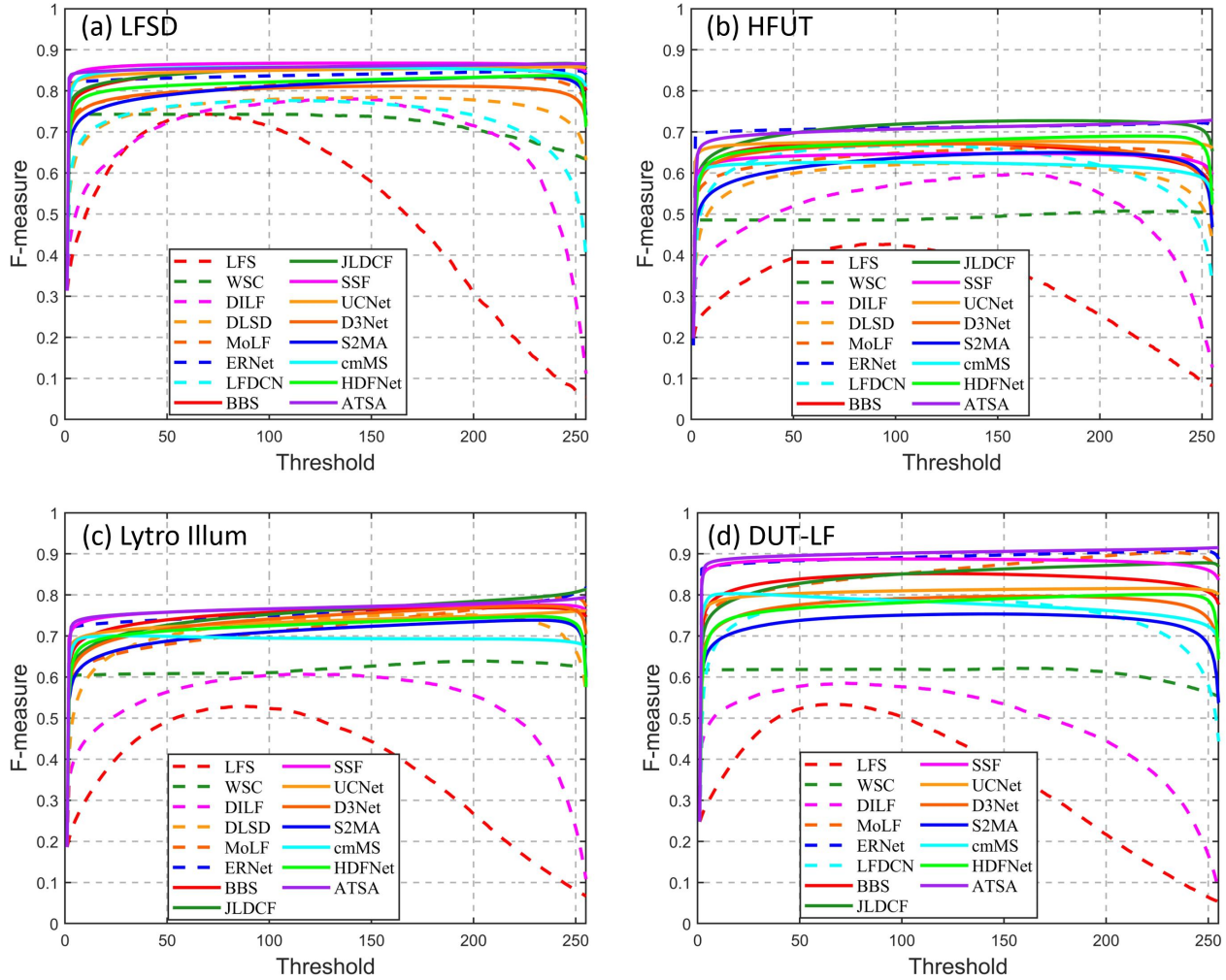


Fig. 13: F-measure curves under different thresholds on four datasets ((a) LFSD [39], (b) HFUT [44], (c) Lytro Illum [52] and (d) DUT-LF [49]) for seven light field SOD models (*i.e.*, LFS [39], WSC [40], DILF [25], DLSD [50], MoLF [26], ERNet [27], LFDCN [52]) and nine SOTA RGB-D based SOD models (*i.e.*, BBS [29], JLDCF [28], SSF [32], UCNet [33], D3Net [34], S2MA [35], cmMS [36], HDFNet [37], and ATSA [30]). Note that in this figure, the *solid lines* and *dashed lines* represent the F-measure curves of *RGB-D based SOD models* and *light field SOD models*, respectively.

aggregation module [30], or UNet-shaped bottom-up/top-down architecture [28], [35], [80] to achieve this goal. In contrast, the field of light field SOD is less explored and the models/architectures evolve slowly. The edge-aware properties are still not yet considered by most of the existing models. Besides, although the attention mechanism and ConvLSTM are adopted by ERNet, no top-down refinement is implemented to generate a saliency map with more accurate boundaries. As evidenced in Fig. 1 and Fig. 14, those RGB-D SOD models tend to detect more accurate boundaries than existing deep light field SOD models. Second, the other potential reason could be that those RGB-D SOD models are trained on more data. For instance, JLDCF was trained on 2200 RGB-D scenarios according to [28], while ERNet [27] was trained only on ~ 1000 light fields. Thus, the former is more likely to obtain better generalizability using the large-scale dataset.

However, although RGB-D models only leverage depth information, which is a subset information of light fields as

we mention before, according to the above findings, we can still hardly deny the potentials of light fields on boosting the performance of SOD, as recently RGB-D SOD area is much more active (many new competitive models are proposed as mentioned in [62]) than the area of light field SOD. Besides, the performance of ERNet and MoLF are only slightly lower than the RGB-D models on the three datasets, which still validates the effectiveness of light fields for SOD [53]. Also, we conclude there is still considerable room for improving the light field SOD, because a light field can provide much more information than a pair of RGB and depth images.

4) *Accuracy across different datasets*: It is clearly shown in Table IV and Fig. 12 that the tested models perform differently on different datasets. Generally, the models achieve better results on LFSD than on the other three datasets, indicating that LFSD is the easiest dataset for light field SOD, on which the traditional model DILF can even outperform some deep models like DLSD and LFDCN. In contrast, HFUT, Lytro

Illum and DUT-LF are more challenging. From Fig. 7, one can also see that except LFS, the other three datasets have limited light field depth ranges. Note that MoLF, ERNet, ATSA behave prominently on DUT-LF probably because they were trained on DUT-LF's training set or training data. Besides, as we mention in Section II-C, HFUT has many small salient objects with multiple objects existed per image. The degraded performance of these models on this dataset tells that detecting small/multiple salient objects is still very challenging for existing techniques, no matter for RGB-D based models or light field models. This makes HFUT the most difficult dataset for SOD among the existing light field datasets.

5) *Results visualization*: Fig. 14 visualizes some sample results from five light field models, including two traditional methods (*i.e.*, LFS and DILF) and three deep learning-based models (*i.e.*, DLSD, MoLF and ERNet), and three latest RGB-D based models (*i.e.*, JLDCF, BBS, and ATSA). The first two rows in Fig. 14 show easy cases while the 3rd to 5th rows show cases with complex background or sophisticated boundaries. The last row gives an example with low color contrast between foreground and background. It can be observed in Fig. 14 that RGB-D models perform comparably or even better than light field models, which confirms the fact that this field is still insufficiently studied. Fig. 15 further shows several scenarios with small and multiple salient objects, where the first three rows show the cases with multiple salient objects and the others show the cases of small objects. According to Fig. 15, both RGB-D based models and light field models are more likely to result in erroneous detection, confirming the challenge of handling small/multiple objects for existing techniques.

IV. CHALLENGES AND OPEN DIRECTIONS

This section provides several future research directions and outlines several open issues.

A. Dataset Collection and Unification

As demonstrated in Section II-C, existing light field datasets are limited in scale and have non-unified data forms, making it difficult to evaluate different models and also to generalize deep networks. This data issue is *practically severe* for light field SOD because of its diverse data representations and high dependency on special acquisition hardware, differing it from other SOD tasks (*e.g.*, RGB-D SOD [28], [30], [32], video SOD [81], [82]) in the saliency community. Therefore, some large-scale and unified datasets are essential for future research. We suggest those researchers who are going to construct new light field SOD datasets to elegantly take this issue into consideration. Providing complete data forms including raw data, focal stacks, multi-view images, depth maps, and micro-lens image arrays would definitely facilitate and advance the research on this topic. However, we also note there is a challenge of data storage and transmission, since the raw light field data is quite large in size (*e.g.*, 640 light fields of Lytro Illum occupy 32.8 Gigabytes), not to say together with other off-the-shelf data forms, making the entire dataset a bit difficult to spread. Anyway, it will still be great if a subset of any specific data form is available for public.

B. Further Investigation Needed in Light Field SOD

As surveyed, till now, there are fewer studies regarding SOD on light fields compared to other areas in the saliency community. Thus, this field is still less active and under-explored. Also, from the benchmarking results in Section III-C, we can conclude that the SOTA performance is still far from satisfactory, especially on HFUT dataset. Considerable room exists for further improvement on algorithms/models. Also note that regarding models using modern deep learning techniques, there are only six models emerging in 2019 and 2020. We attribute such scarce research works on light field SOD to the data issue mentioned above and also the lack of a complete survey of existing methods and datasets on this topic, which is rightly the goal of this paper.

C. Multi-view Images and Micro-lens Image Arrays

Most existing models work with focal stacks and depth as surveyed in Table I, while multi-view images and micro-lens image arrays are two other types of light field data representations which are seldom considered (only four related models). The benchmarking results in Section III-C imply that the related models perform less better than models utilizing other data forms, so the utilization of these two data forms is still insufficiently explored. More new models are expected in the future to explore the effectiveness of multi-view images and micro-lens image arrays for light field SOD. Another potential reason could be that, these two data forms themselves may be less information-representative than focal stacks and depth maps, namely scene depth information is conveyed more implicitly. This could let finding effective mappings and mining underlying rules using deep neural networks difficult, especially when the training data is sparse. In addition, the comparison between different data forms on the effectiveness and redundancy for saliency detection is an interesting work.

D. Incorporating High-quality Depth Estimation

It has been proven that accurate depth maps are conducive to discovering salient objects from complex background. Unfortunately, the quality of provided depth maps right now vary greatly, because depth estimation from light field is a challenging problem [55]–[58], easily leading to imperfect depth. The challenge is due to the fact that although the light field can synthesize images focusing at any depth by using digital refocusing techniques, the depth assignment of each scene point is unknown and resorts to the judgement of if an image region is in-focus, which itself is an open problem [83], [84]. Imperfect depth maps often result in negative effect on detection accuracy for models using depth maps. Therefore, incorporating high-quality depth estimation algorithms from light field is for sure beneficial for boosting performance.

E. Edge-aware Light Field SOD

Accurate object boundaries are essential for high quality saliency maps, as SOD itself is a pixel-wise segmentation task [4]. In the RGB SOD field, edge-aware SOD models are drawing increasing research attention [77]–[79]. Currently, as

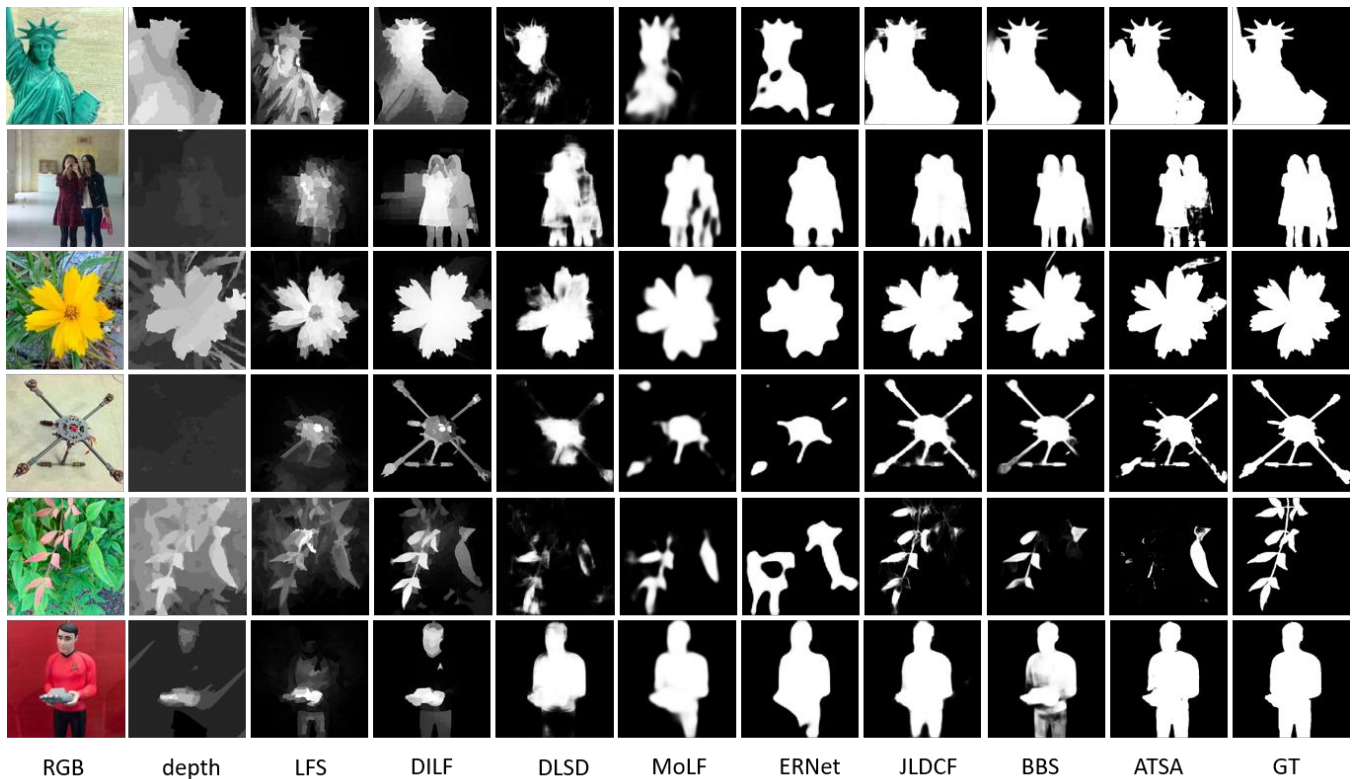


Fig. 14: Visual comparison for five light field SOD (*i.e.*, LFS [39], DILF [25], DLSD [50], MoLF [26] and ERNet [27]) and three SOTA RGB-D based SOD models (*i.e.*, JLDCF [28], BBS [29], and ATSA [30]).

shown through our experimental results, existing deep light field SOD models seldom consider this issue and obtain saliency results with coarse boundaries/edges, implying that edge-aware light field SOD could be a future direction.

F. Development of Acquisition Technology and Hardware

As we mentioned before, the first generation light field camera named Lytro was invented in 2011, while its successor called Lytro Illum came in 2014. The latter is more powerful but has a much large size than the former and is also much more cost expensive. However, generally speaking, the development of acquisition technology and hardware of light field is slow comparing to other IT areas such as computers and mobile phones, because after 2014, very few commercial light field cameras are announced. Therefore technology development on acquisition and hardware is urgently required for light field photography. Currently, regarding no matter photographing quality, as well as price and portability, light field cameras still cannot take the place of the conventional RGB cameras. Imagining that in the future if the light field cameras become affordable and small in size, which can easily be integrated into our mobile phones, everyone can try light field photographing in our daily life. There will be increasing vast amount of user data and post-processing application requirements, on which light field SOD then can play a role and be driven a long way.

G. Link RGB-D SOD to Light Field SOD

There is indeed a close connection between light field SOD and RGB-D SOD, since both tasks often explore scene depth information for saliency detection, whereas depth information can be derived from light field data via different techniques. That is why RGB-D SOD could be deemed as a degenerated solution for tackling light field SOD. As shown in Table IV, applying RGB-D SOD models to light field is straightforward, whereas its reverse we believe could also be possible. For example, intuitively, reconstructing light field data such as focal stacks or multi-view images from a pair of RGB and depth images is possible (*e.g.*, [50]). If this bridge is achieved, mutual transfer between the models of these two fields becomes feasible, and light field models then can also be applied to RGB-D data. Such a link must be an interesting issue to explore in the near future.

H. Different Supervision Strategies

Existing deep light field models learn to segment salient objects in a fully supervised strategy, which demands sufficient annotated training data. Unfortunately, as mentioned before, existing datasets are limited in scale, *e.g.*, DUT-LF and DUT-MV provide 1000 and 1100 samples for training, respectively, while other datasets contain light fields fewer than 640. On one hand, small training data limits the generalization ability of models. On the other hand, large amount of annotated data contradictorily requires massive manual effort on data collection and labeling. Recently, weakly and semi-supervised

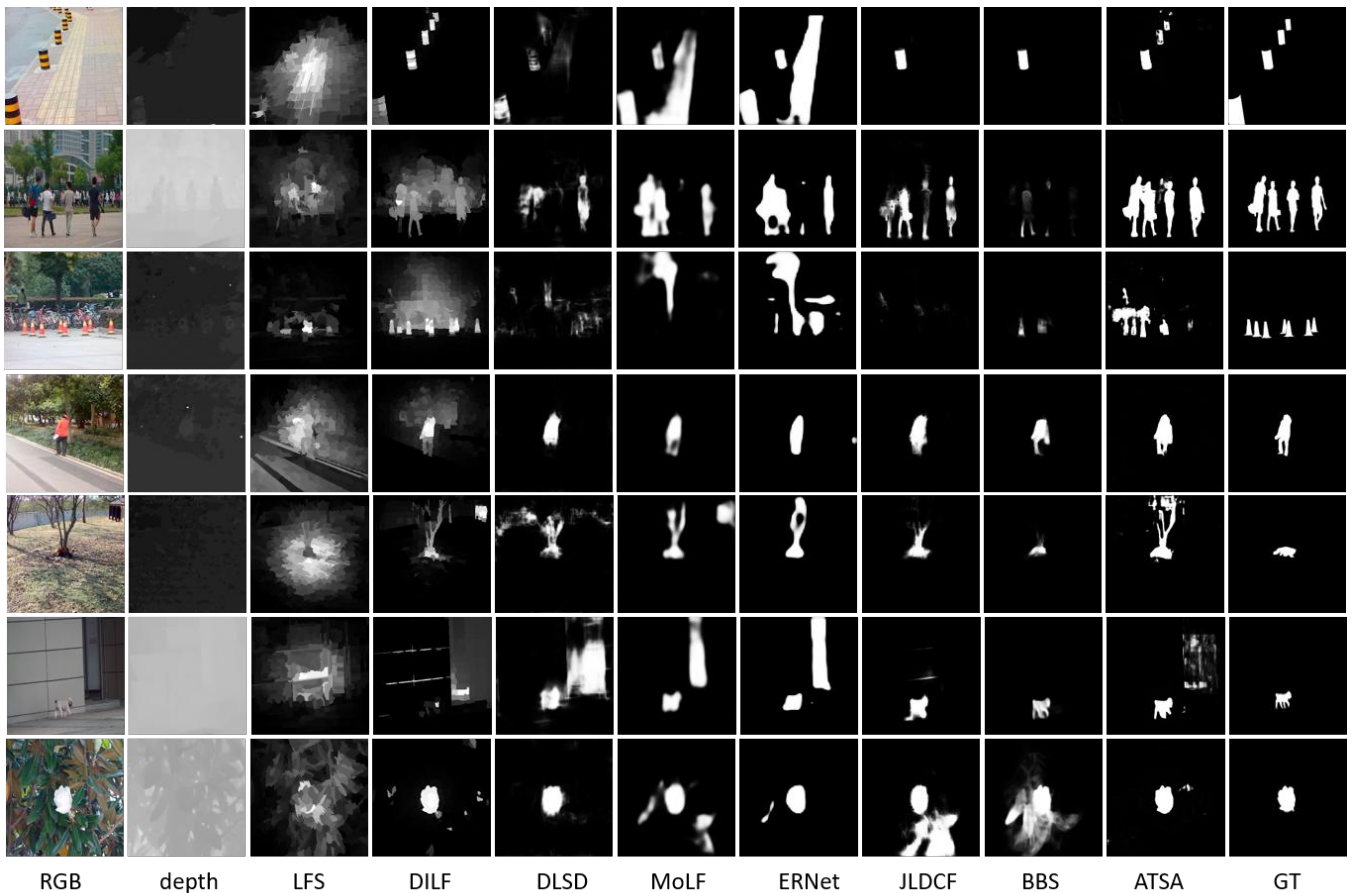


Fig. 15: Visual comparison of five light field SOD (*i.e.*, LFS [39], DILF [25], DLSD [50], MoLF [26] and ERNet [27]) and three SOTA RGB-D based SOD models (*i.e.*, JLDCF [28], BBS [29], and ATSA [30]) on detecting small and multiple objects.

learning strategies have drawn extensive research attention, largely reducing the annotation effort. Because of being data-friendly, they have been introduced to RGB SOD and some encouraging attempts [8], [85], [86] have been made. Inspired by this, one future direction is to extend these supervision strategies to light field SOD for overcoming the shortage of training data. Additionally, several works [87], [88] have proven that pre-training models in a self-supervision manner can effectively improve the performance, which can also be introduced to light field SOD in the future.

I. Other Potential Directions

There may also be other potential directions inspired by the recent advances in the saliency community. For example, high-resolution salient object detection [89] aims to handle salient object segmentation in high-resolution images, thus achieving high-resolution details could be considered in light field SOD. Besides, existing light field datasets are labeled in object-level, while instance-level annotation and detection aims at separating individual objects as in [90]–[93], can also be introduced into this field. Note that there are quite some instance-sensitive application scenarios, *e.g.*, image captioning [94], multi-label image recognition [95] as well as various weakly supervised/unsupervised learning scenarios [96], [97]. A recent work attempts to address weakly-supervised salient

instance detection [98]. Therefore, more effort may be spent on instance-level ground-truth annotation and designing instance-level light field SOD models. Furthermore, as we know eye-fixation prediction [3]–[5] is another sub-field of saliency detection. Till now no research is about eye-fixation prediction on light field data. As abundant nature scene information is provided by light field, we hope that the various data forms of light field provide useful cues to help eliminate ambiguous human attention. Lastly, light field data could benefit other closely related tasks to SOD, such as camouflaged object detection (COD) [99] and transparent object segmentation [100], where objects often borrow texture from their background and have similar appearances to their surroundings.

Besides, there is an unanswered question that: *how light field information can benefit SOD over depth information*. As we know, depth information can be derived from and is a subset of light field data. Different light field data forms, *e.g.*, focal stacks and multi-view images, somewhat imply depth information, indicating that existing models may leverage such depth information in an implicit way. So how is the gap between using depth in an explicit way (like RGB-D SOD models do) and in an implicit way? This is an interesting question, but unfortunately since the problem of light field SOD was proposed in 2014, no any study showed any direct answer/evidence. Such an answer deserves further investigation and understanding into this field in the future.

V. CONCLUSION

We provide the first comprehensive review and benchmark for light field SOD, where we review existing studies and related datasets. We have benchmarked representative light field SOD models and compared them to several cutting-edge RGB-D SOD models both qualitatively and quantitatively. Considering the fact that the existing light field datasets are somewhat inconsistent in data forms, we propose to generate more data from existing datasets as supplement, making them more complete and unified. Moreover, we discuss several potential directions for future research and outline some open issues. Although progress have been made over the past six years, there are only six deep learning-based works focusing on this topic, leaving significant room to design more powerful network architectures and incorporate effective modules (*e.g.*, edge-aware potentials and top-down refinement) for improving SOD performance. We hope this survey, together with its released materials, could serve as a catalyst to advance this area and promote interesting works in the future.

REFERENCES

- [1] M.-M. Cheng, G.-X. Zhang, N. Mitra, X. Huang, and S. Hu, "Global contrast based salient region detection," in *Proceedings of the IEEE Conference on Computer Vision and Pattern Recognition*, 2011, pp. 409–416.
- [2] A. Borji, D. N. Sihite, and L. Itti, "Quantitative analysis of human-model agreement in visual saliency modeling: A comparative study," *IEEE Transactions on Image Processing*, vol. 22, pp. 55–69, 2013.
- [3] A. Borji, "Saliency prediction in the deep learning era: Successes and limitations," *IEEE Transactions on Pattern Analysis and Machine Intelligence*, 2019.
- [4] A. Borji, M. Cheng, H. Jiang, and J. Li, "Salient object detection: A benchmark," *IEEE Transactions on Image Processing*, vol. 24, pp. 5706–5722, 2015.
- [5] A. Borji and L. Itti, "State-of-the-art in visual attention modeling," *IEEE Transactions on Pattern Analysis and Machine Intelligence*, vol. 35, pp. 185–207, 2013.
- [6] G. Liu and D. Fan, "A model of visual attention for natural image retrieval," in *Proceedings of the IEEE Conference on Information Science and Cloud Computing Companion*. IEEE, 2013, pp. 728–733.
- [7] Z. Ren, S. Gao, L. Chia, and I. Tsang, "Region-based saliency detection and its application in object recognition," *IEEE Transactions on Circuits and Systems for Video Technology*, vol. 24, pp. 769–779, 2014.
- [8] D. Zhang, D. Meng, L. Zhao, and J. Han, "Bridging saliency detection to weakly supervised object detection based on self-paced curriculum learning," in *Proceedings of the International Joint Conferences on Artificial Intelligence*, 2016.
- [9] U. Rutishauser, D. B. Walther, C. Koch, and P. Perona, "Is bottom-up attention useful for object recognition?" in *Proceedings of the IEEE Conference on Computer Vision and Pattern Recognition*, 2004.
- [10] F. Moosmann, D. Larlus, and F. Jurie, "Learning saliency maps for object categorization," in *Eccv International Workshop on the Representation & Use of Prior Knowledge in Vision*, 2006.
- [11] Y. Wei, J. Feng, X. Liang, M.-M. Cheng, Y. Zhao, and S. Yan, "Object region mining with adversarial erasing: A simple classification to semantic segmentation approach," in *Proceedings of the IEEE Conference on Computer Vision and Pattern Recognition*, 2017, pp. 6488–6496.
- [12] Y. Wei, X. Liang, Y. Chen, X. Shen, M.-M. Cheng, Y. Zhao, and S. Yan, "Stc: A simple to complex framework for weakly-supervised semantic segmentation," *IEEE Transactions on Pattern Analysis and Machine Intelligence*, vol. 39, pp. 2314–2320, 2017.
- [13] X. Wang, S. You, X. Li, and H. Ma, "Weakly-supervised semantic segmentation by iteratively mining common object features," in *Proceedings of the IEEE Conference on Computer Vision and Pattern Recognition*, 2018, pp. 1354–1362.
- [14] W. Wang, J. Shen, R. Yang, and F. Porikli, "Saliency-aware video object segmentation," *IEEE Transactions on Pattern Analysis and Machine Intelligence*, vol. 40, pp. 20–33, 2018.
- [15] H. Song, W. Wang, S. Zhao, J. Shen, and K. Lam, "Pyramid dilated deeper convlstm for video salient object detection," in *Proceedings of the European Conference on Computer Vision*, 2018.
- [16] J. Han, E. J. Pauwels, and P. M. de Zeeuw, "Fast saliency-aware multi-modality image fusion," *Neurocomputing*, vol. 111, pp. 70–80, 2013.
- [17] W. Wang, J. Shen, and H. Ling, "A deep network solution for attention and aesthetics aware photo cropping," *IEEE Transactions on Pattern Analysis and Machine Intelligence*, vol. 41, pp. 1531–1544, 2019.
- [18] J. Sun and H. Ling, "Scale and object aware image retargeting for thumbnail browsing," in *Proceedings of the IEEE International Conference on Computer Vision*, 2011, pp. 1511–1518.
- [19] Y.-F. Ma, L. Lu, H. Zhang, and M. Li, "A user attention model for video summarization," in *MULTIMEDIA '02*, 2002.
- [20] D. Simakov, Y. Caspi, E. Shechtman, and M. Irani, "Summarizing visual data using bidirectional similarity," *Proceedings of the IEEE Conference on Computer Vision and Pattern Recognition*, pp. 1–8, 2008.
- [21] Y. Sugano, Y. Matsushita, and Y. Sato, "Calibration-free gaze sensing using saliency maps," in *Proceedings of the IEEE Conference on Computer Vision and Pattern Recognition*, 2010, pp. 2667–2674.
- [22] A. Borji and L. Itti, "Defending yabus: eye movements reveal observers' task," *Journal of vision*, vol. 14 3, p. 29, 2014.
- [23] A. Karpathy, S. Miller, and L. Fei-Fei, "Object discovery in 3d scenes via shape analysis," *2013 IEEE International Conference on Robotics and Automation*, pp. 2088–2095, 2013.
- [24] S. Frintrop, G. M. García, and A. B. Cremers, "A cognitive approach for object discovery," *2014 22nd International Conference on Pattern Recognition*, pp. 2329–2334, 2014.
- [25] J. Zhang, M. Wang, J. Gao, Y. Wang, X. Zhang, and X. Wu, "Saliency detection with a deeper investigation of light field," in *Proceedings of the International Joint Conferences on Artificial Intelligence*, 2015.
- [26] M. Zhang, J. Li, J. Wei, Y. Piao, and H. Lu, "Memory-oriented decoder for light field salient object detection," in *Proceedings of the Advances in Neural Information Processing Systems*, 2019.
- [27] Y. Piao, Z. Rong, M. Zhang, and H. Lu, "Exploit and replace: An asymmetrical two-stream architecture for versatile light field saliency detection," in *AAAI*, 2020.
- [28] K. Fu, D.-P. Fan, G.-P. Ji, and Q. Zhao, "Jl-dcf: Joint learning and densely-cooperative fusion framework for rgb-d salient object detection," in *Proceedings of the IEEE Conference on Computer Vision and Pattern Recognition*, 2020, pp. 3049–3059.
- [29] D.-P. Fan, Y. Zhai, A. Borji, J. Yang, and L. Shao, "Bbs-net: Rgb-d salient object detection with a bifurcated backbone strategy network," in *Proceedings of the European Conference on Computer Vision*, vol. abs/2007.02713, 2020.
- [30] M. Zhang, S. X. Fei, J. Liu, S. Xu, Y. Piao, and H. Lu, "Asymmetric two-stream architecture for accurate rgb-d saliency detection," in *Proceedings of the European Conference on Computer Vision*, 2020.
- [31] D.-P. Fan, M.-M. Cheng, J.-J. Liu, S.-H. Gao, Q. Hou, and A. Borji, "Salient objects in clutter: Bringing salient object detection to the foreground," in *Proceedings of the Conference on European conference on computer vision*, 2018, pp. 186–202.
- [32] M. Zhang, W. Ren, Y. Piao, Z. Rong, and H. Lu, "Select, supplement and focus for rgb-d saliency detection," in *Proceedings of the IEEE Conference on Computer Vision and Pattern Recognition*, 2020, pp. 3469–3478.
- [33] J. Zhang, D.-P. Fan, Y. Dai, S. Anwar, F. S. Saleh, T. Zhang, and N. Barnes, "Uc-net: Uncertainty inspired rgb-d saliency detection via conditional variational autoencoders," in *Proceedings of the IEEE Conference on Computer Vision and Pattern Recognition*, 2020, pp. 8579–8588.
- [34] D.-P. Fan, Z. Lin, J. Zhao, Y. Liu, Z. Zhang, Q. Hou, M. Zhu, and M.-M. Cheng, "Rethinking rgb-d salient object detection: Models, datasets, and large-scale benchmarks," *IEEE Transactions on Neural Networks and Learning Systems*, vol. PP, 2020.
- [35] N. Liu, N. Zhang, and J. Han, "Learning selective self-mutual attention for rgb-d saliency detection," in *Proceedings of the IEEE Conference on Computer Vision and Pattern Recognition*, 2020, pp. 13 753–13 762.
- [36] C. Li, R. Cong, Y. Piao, Q. Xu, and C. C. Loy, "Rgb-d salient object detection with cross-modality modulation and selection," in *Proceedings of the European Conference on Computer Vision*, vol. abs/2007.07051, 2020.

- [37] Y. Pang, L. Zhang, X.-Q. Zhao, and H. Lu, "Hierarchical dynamic filtering network for rgb-d salient object detection," in *Proceedings of the European Conference on Computer Vision*, vol. abs/2007.06227, 2020.
- [38] H.-F. Li, G. Chen, G. Li, and Y. Yu, "Motion guided attention for video salient object detection," in *Proceedings of the IEEE International Conference on Computer Vision*, 2019, pp. 7273–7282.
- [39] N. Li, J. Ye, Y. Ji, H. Ling, and J. Yu, "Saliency detection on light field," in *Proceedings of the IEEE Conference on Computer Vision and Pattern Recognition*, 2014, pp. 2806–2813.
- [40] N. Li, B. Sun, and J. Yu, "A weighted sparse coding framework for saliency detection," in *Proceedings of the IEEE Conference on Computer Vision and Pattern Recognition*, 2015, pp. 5216–5223.
- [41] H. Sheng, S. Zhang, X. Liu, and Z. Xiong, "Relative location for light field saliency detection," in *Proceedings of the IEEE International Conference on Acoustics, Speech and Signal Processing*, 2016, pp. 1631–1635.
- [42] A. Wang, M. Wang, X. Li, Z. Mi, and H. Zhou, "A two-stage bayesian integration framework for salient object detection on light field," *Neural Processing Letters*, vol. 46, pp. 1083–1094, 2017.
- [43] N. Li, J. Ye, Y. Ji, H. Ling, and J. Yu, "Saliency detection on light field," *IEEE Transactions on Pattern Analysis and Machine Intelligence*, vol. 39, no. 8, pp. 1605–1616, 2017.
- [44] J. Zhang, M. Wang, L. Lin, X. Yang, J. Gao, and Y. Rui, "Saliency detection on light field: A multi-cue approach," *ACM Transactions on Multimedia Computing, Communications*, vol. 13, pp. 1–12, 2017.
- [45] H. Wang, B. Yan, X. Wang, Y. Zhang, and Y. Yang, "Accurate saliency detection based on depth feature of 3d images," *Multimedia Tools and Applications*, vol. 77, no. 12, pp. 14 655–14 672, 2018.
- [46] S. Wang, W. Liao, P. Surman, Z. Tu, Y. Zheng, and J. Yuan, "Saliency guided depth calibration for perceptually optimized compressive light field 3d display," in *Proceedings of the IEEE Conference on Computer Vision and Pattern Recognition*, 2018, pp. 2031–2040.
- [47] X. Wang, Y. Dong, Q. Zhang, and Q. Wang, "Region-based depth feature descriptor for saliency detection on light field," *Multimedia Tools and Applications*, pp. 1–18, 2020.
- [48] Y. Piao, X. chun Li, M. Zhang, J. Yu, and H. Lu, "Saliency detection via depth-induced cellular automata on light field," *IEEE Transactions on Image Processing*, vol. 29, pp. 1879–1889, 2020.
- [49] T. Wang, Y. Piao, H. Lu, X. chun Li, and L. Zhang, "Deep learning for light field saliency detection," in *Proceedings of the IEEE International Conference on Computer Vision*, 2019, pp. 8837–8847.
- [50] Y. Piao, Z. Rong, M. Zhang, X. Li, and H. Lu, "Deep light-field-driven saliency detection from a single view," in *Proceedings of the International Joint Conferences on Artificial Intelligence*, 2019.
- [51] M. Zhang, W. Ji, Y. Piao, J. Li, Y. Zhang, S. Xu, and H. Lu, "Lfnnet: Light field fusion network for salient object detection," *IEEE Transactions on Image Processing*, vol. 29, pp. 6276–6287, 2020.
- [52] J. Zhang, Y. Liu, S. Zhang, R. Poppe, and M. Wang, "Light field saliency detection with deep convolutional networks," *IEEE Transactions on Image Processing*, vol. 29, pp. 4421–4434, 2020.
- [53] X. Zhang, Y. Wang, J. Zhang, L. Hu, and M. Wang, "Light field saliency vs. 2d saliency: A comparative study," *Neurocomputing*, vol. 166, pp. 389–396, 2015.
- [54] A. Gershun, "The light field," *Studies in Applied Mathematics*, vol. 18, no. 1-4, p. 51–151, 1939.
- [55] H. Jeon, J. Park, G. Choe, J. Park, Y. Bok, Y.-W. Tai, and I.-S. Kweon, "Accurate depth map estimation from a lenslet light field camera," in *Proceedings of the IEEE Conference on Computer Vision and Pattern Recognition*, 2015, pp. 1547–1555.
- [56] M. W. Tao, S. Hadap, J. Malik, and R. Ramamoorthi, "Depth from combining defocus and correspondence using light-field cameras," in *Proceedings of the IEEE International Conference on Computer Vision*, 2013, pp. 673–680.
- [57] M. W. Tao, P. P. Srinivasan, J. Malik, S. Rusinkiewicz, and R. Ramamoorthi, "Depth from shading, defocus, and correspondence using light-field angular coherence," in *Proceedings of the IEEE Conference on Computer Vision and Pattern Recognition*, 2015, pp. 1940–1948.
- [58] T. Wang, A. A. Efros, and R. Ramamoorthi, "Occlusion-aware depth estimation using light-field cameras," in *Proceedings of the IEEE International Conference on Computer Vision*, 2015, pp. 3487–3495.
- [59] R. Ng, M. Levoy, M. Brédif, G. Duval, M. Horowitz, and P. Hanrahan, "Light field photography with a hand-held plenoptic camera," *Technical Report CTSR 2005-02*, vol. CTSR, 01 2005.
- [60] P. Jiang, H. Ling, J. Yu, and J. Peng, "Salient region detection by ufo: Uniqueness, focusness and objectness," in *Proceedings of the IEEE International Conference on Computer Vision*, 2013, pp. 1976–1983.
- [61] C. Buehler, M. Bosse, L. McMillan, S. Gortler, and M. Cohen, "Unstructured lumigraph rendering," in *SIGGRAPH '01*, 2001.
- [62] T. Zhou, D.-P. Fan, M.-M. Cheng, J. Shen, and L. Shao, "Rgb-d salient object detection: A survey," *Computational Visual Media*, 2020.
- [63] E. Adelson and J. Bergen, "The plenoptic function and the elements of early vision," in *Computational Models of Visual Processing*. Cambridge: MIT Press, 1991.
- [64] M. Levoy and P. Hanrahan, "Light field rendering," in *SIGGRAPH '96*, 1996.
- [65] A. Agarwala, M. Dontcheva, M. Agrawala, S. Drucker, A. Colburn, B. Curless, D. Salesin, and M. Cohen, "Interactive digital photomontage," in *SIGGRAPH 2004*, 2004.
- [66] X. Lin, J.-L. Suo, G. Wetzstein, Q. Dai, and R. Raskar, "Coded focal stack photography," *Proceedings of the IEEE Conference on Computational Photography*, pp. 1–9, 2013.
- [67] W. Zhu, S. Liang, Y. Wei, and J. Sun, "Saliency optimization from robust background detection," in *Proceedings of the IEEE Conference on Computer Vision and Pattern Recognition*, 2014, pp. 2814–2821.
- [68] X. Shi, Z. Chen, H. Wang, D. Yeung, W. Wong, and W. Woo, "Convolutional lstm network: a machine learning approach for precipitation nowcasting," in *Proceedings of the Advances in Neural Information Processing Systems*, 2015, pp. 802–810.
- [69] L.-C. Chen, G. Papandreou, I. Kokkinos, K. Murphy, and A. Yuille, "Deeplab: Semantic image segmentation with deep convolutional nets, atrous convolution, and fully connected crfs," *IEEE Transactions on Pattern Analysis and Machine Intelligence*, vol. 40, pp. 834–848, 2018.
- [70] C. Yang, L. Zhang, H. Lu, X. Ruan, and M.-H. Yang, "Saliency detection via graph-based manifold ranking," in *Proceedings of the IEEE Conference on Computer Vision and Pattern Recognition*, 2013, pp. 3166–3173.
- [71] L. Wang, H. Lu, Y. Wang, M. Feng, D. Wang, B. Yin, and X. Ruan, "Learning to detect salient objects with image-level supervision," in *Proceedings of the IEEE Conference on Computer Vision and Pattern Recognition*, 2017, pp. 3796–3805.
- [72] R. Achanta, S. Hemami, F. J. Estrada, and S. Süsstrunk, "Frequency-tuned salient region detection," in *Proceedings of the IEEE Conference on Computer Vision and Pattern Recognition*, 2009.
- [73] F. Perazzi, P. Krähenbühl, Y. Pritch, and A. Sorkine-Hornung, "Saliency filters: Contrast based filtering for salient region detection," in *Proceedings of the IEEE Conference on Computer Vision and Pattern Recognition*, 2012, pp. 733–740.
- [74] D.-P. Fan, M.-M. Cheng, Y. Liu, T. Li, and A. Borji, "Structure-measure: A new way to evaluate foreground maps," in *Proceedings of the IEEE International Conference on Computer Vision*, 2017, pp. 4558–4567.
- [75] J. Zhao, Y. Cao, D.-P. Fan, M.-M. Cheng, X. yi Li, and L. Zhang, "Contrast prior and fluid pyramid integration for rgb-d salient object detection," in *Proceedings of the IEEE Conference on Computer Vision and Pattern Recognition*, 2019, pp. 3922–3931.
- [76] D.-P. Fan, C. Gong, Y. Cao, B. Ren, M.-M. Cheng, and A. Borji, "Enhanced-alignment measure for binary foreground map evaluation," in *Proceedings of the International Joint Conferences on Artificial Intelligence*, 2018.
- [77] Z. Wu, L. Su, and Q. Huang, "Stacked cross refinement network for edge-aware salient object detection," in *Proceedings of the IEEE International Conference on Computer Vision*, 2019, pp. 7263–7272.
- [78] M. Feng, H. Lu, and E. Ding, "Attentive feedback network for boundary-aware salient object detection," in *Proceedings of the IEEE Conference on Computer Vision and Pattern Recognition*, 2019, pp. 1623–1632.
- [79] X. Qin, Z. Zhang, C. Huang, C. Gao, M. Dehghan, and M. Jägersand, "Basnet: Boundary-aware salient object detection," in *Proceedings of the IEEE Conference on Computer Vision and Pattern Recognition*, 2019, pp. 7471–7481.
- [80] G. Li, Z. Liu, and H. Ling, "Icnet: Information conversion network for rgb-d based salient object detection," *IEEE Transactions on Image Processing*, vol. 29, pp. 4873–4884, 2020.
- [81] A. Tsiami, P. Koutras, and P. Maragos, "Stavis: Spatio-temporal audio-visual saliency network," in *Proceedings of the IEEE Conference on Computer Vision and Pattern Recognition*, 2020, pp. 4765–4775.
- [82] D.-P. Fan, W. Wang, M.-M. Cheng, and J. Shen, "Shifting more attention to video salient object detection," in *Proceedings of the IEEE Conference on Computer Vision and Pattern Recognition*, 2019, pp. 8546–8556.
- [83] W. Zhao, F. Zhao, D. Wang, and H. Lu, "Defocus blur detection via multi-stream bottom-top-bottom network," *IEEE Transactions on*

- Pattern Analysis and Machine Intelligence*, vol. 42, pp. 1884–1897, 2020.
- [84] J. Park, Y.-W. Tai, D. Cho, and I.-S. Kweon, “A unified approach of multi-scale deep and hand-crafted features for defocus estimation,” in *Proceedings of the IEEE Conference on Computer Vision and Pattern Recognition*, 2017, pp. 2760–2769.
- [85] Y. Zeng, Y.-Z. Zhuge, H. Lu, L. Zhang, M. Qian, and Y. Yu, “Multi-source weak supervision for saliency detection,” in *Proceedings of the IEEE Conference on Computer Vision and Pattern Recognition*, 2019, pp. 6067–6076.
- [86] M. Qian, J. Qi, L. Zhang, M. Feng, and H. Lu, “Language-aware weak supervision for salient object detection,” *Pattern Recognit.*, vol. 96, 2019.
- [87] T. Chen, S. Liu, S. Chang, Y. Cheng, L. Amini, and Z. Wang, “Adversarial robustness: From self-supervised pre-training to fine-tuning,” in *Proceedings of the IEEE Conference on Computer Vision and Pattern Recognition*, 2020, pp. 696–705.
- [88] A. Dai, C. Diller, and M. Nießner, “Sg-nn: Sparse generative neural networks for self-supervised scene completion of rgb-d scans,” in *Proceedings of the IEEE Conference on Computer Vision and Pattern Recognition*, 2020, pp. 846–855.
- [89] Y. Zeng, P. Zhang, J. Zhang, Z. Lin, and H. Lu, “Towards high-resolution salient object detection,” in *Proceedings of the IEEE International Conference on Computer Vision*, 2019, pp. 7233–7242.
- [90] Z. Cai and N. Vasconcelos, “Cascade r-cnn: High quality object detection and instance segmentation,” *IEEE Transactions on Pattern Analysis and Machine Intelligence*, 2019.
- [91] K. Chen, J. Pang, J. Wang, Y. Xiong, X. Li, S. Sun, W. Feng, Z. Liu, J. Shi, W. Ouyang, C. C. Loy, and D. Lin, “Hybrid task cascade for instance segmentation,” in *Proceedings of the IEEE Conference on Computer Vision and Pattern Recognition*, 2019, pp. 4969–4978.
- [92] S. Liu, L. Qi, H. Qin, J. Shi, and J. Jia, “Path aggregation network for instance segmentation,” in *Proceedings of the IEEE Conference on Computer Vision and Pattern Recognition*, 2018, pp. 8759–8768.
- [93] G. Li, Y. Xie, L. Lin, and Y. Yu, “Instance-level salient object segmentation,” in *Proceedings of the IEEE Conference on Computer Vision and Pattern Recognition*, 2017, pp. 247–256.
- [94] A. Karpathy and F.-F. Li, “Deep visual-semantic alignments for generating image descriptions,” *IEEE Transactions on Pattern Analysis and Machine Intelligence*, vol. 39, pp. 664–676, 2017.
- [95] Y. Wei, W. Xia, J. Huang, B. Ni, J. Dong, Y. Zhao, and S. Yan, “Cnn: Single-label to multi-label,” *ArXiv*, vol. abs/1406.5726, 2014.
- [96] X. Chen and A. Gupta, “Weakly supervised learning of convolutional networks,” in *Proceedings of the IEEE International Conference on Computer Vision*, 2015, pp. 1431–1439.
- [97] B. Lai and X. Gong, “Saliency guided dictionary learning for weakly-supervised image parsing,” in *Proceedings of the IEEE Conference on Computer Vision and Pattern Recognition*, 2016, pp. 3630–3639.
- [98] X. Tian, K. Xu, X. Yang, B. Yin, and R. Lau, “Weakly-supervised salient instance detection,” in *Proceedings of the Conference on British Machine Vision Conference*, vol. abs/2009.13898, 2020.
- [99] D.-P. Fan, G.-P. Ji, G. Sun, M.-M. Cheng, J. Shen, and L. Shao, “Camouflaged object detection,” in *Proceedings of the IEEE Conference on Computer Vision and Pattern Recognition*, 2020, pp. 2774–2784.
- [100] Y. Xu, H. Nagahara, A. Shimada, and R. Taniguchi, “Transcut: Transparent object segmentation from a light-field image,” in *Proceedings of the IEEE International Conference on Computer Vision*, 2015, pp. 3442–3450.